2019

Cell Type and Substrate Dependence of Fibronectin Properties and Mechanotransduction

Navpreet S. Saini
Virginia Commonwealth University

Cell Type and Substrate Dependence of Fibronectin Properties and Mechanotransduction

A thesis submitted in partial fulfillment of the requirement for the degree of (Master of Science) in Biomedical Engineering at Virginia Commonwealth University.

by

Navpreet Singh Saini
Bachelor of Science in Bioinformatics, Virginia Commonwealth University, 2016

Adviser: Dr. Seth Weinberg, Ph.D.
Assistant Professor, Biomedical Engineering

Virginia Commonwealth University
Richmond, Virginia
May 2019

Acknowledgements

I would first like to thank my thesis advisor Dr. Seth Weinberg of the Biomedical Engineering program at VCU. I would like to thank him for giving me the opportunity to work with him and helping me to learn in areas that I was not well-versed in. He helped with the finer points in my research and gave me advice on how to professionally work and write in the post-graduate world of research.

I would also like to thank the Director of the Biomedical Engineering program, Dr. Christopher Lemmon, for helping me meet and become a student researcher for Dr. Weinberg. Dr. Lemmon helped me a lot in getting me through my final years as a Master's Student at VCU. He steered me in the right direction in order for me to Graduate on time and with confidence.

I would also like to thank Dr. Angela Reynolds from the Department of Mathematics and Applied Mathematics at VCU. I would like to thank her for willing to serve on my committee on short notice as well as providing feedback to my research.

I would also like to thank my friend, Dr. Berhanu Tameru of the Center for Computational Epidemiology of Tuskegee University. He helped to teach me the syntax and the coding language of MATLAB, which was a crucial part of my research. Without his help, I would not have been able to finish my work with ease.

Tables of Contents

List of Abbreviations

FN: Fibronectin

ECM: Extracellular Matrix

nFN: number of Fibronectin Molecules

Tot Clutch: Total Number of Clutches (Integrin Bonds)

Frac Clutch: Fraction Number of Clutches (Integrin Bonds)

Vu: Velocity of the Fibronectin Fibrils

Ksub: Stiffness of the Cell Substrate

Fsub: Force of the Substrate

SR Ratio: Stretched to Relaxed Length Ratio

LT Ratio: Length to Thickness Ratio

FA: Focal Adhesion

X: Change in Fibril Stretch (Difference between Relaxed Length and Stretched Length)

NM: Number of Myosin Motors

SSF: Stably Stretched Fibrils

FSF: Fluctuating Stretched Fibrils

SF: Stretched Fibrils for the Combined SSF and FSF Fibril Types

List of Figures

List of Equations

Abstract

Fibronectin is an important protein that is able to bind to other fibronectin molecules and to cell surface receptors. In doing so, the interactions fibronectin can perform is important for the processes of cell migration and tissue formation. Understanding the properties of fibronectin and fibril assembly is undeniably useful for areas such as wound healing, where fibronectin molecules are assembled to protect the tissue and to perform other meaningful tasks. Because of these reasons, it is important to understand how fibronectin is assembled and how its properties affect the fibril assembly, which in return affects the way the cell matrix operates. Previously published papers illustrate that the properties of fibronectin affect the mechanotransduction process, the cell conversion of mechanical stimulus to chemical, and this may lead to various changes of the fibril assembly. However, the question that now comes to focus is what variables affect the fibril assembly? The two main variables that come into question is the substrate stiffness (k_{sub}) (pN/nm) and the actin velocity (Vu) (nm/s) of the cell. In order to test this hypothesis, several fibril assembly simulations were performed via using MATLAB based upon the Weinberg-Mair-Lemmon Fibronectin Model. These simulations were performed by varying the parameters of substrate stiffness and actin velocity which in return affects the various measurements of the fibronectin model, such as stretched length, relaxed length, focal adhesion, etc. In addition to these measurements, fibril simulations where fibril size based on the number of fibronectin molecules were examined as well as simulations comparing terminated and non-terminated fibril assembly properties were tested. Through these various experiments, it was determined that the actin velocity and fibril size had the greatest impacts in affecting the fibronectin's properties and its assembly.

Chapter 1: Introduction

The basic premise of the research is the idea that different cell responses can lead to a wide variety of cellular functions and thereby affecting the tissue. These cell responses can be changed depending upon environmental factors and these responses can alter the way a tissue behaves. The processes of cell differentiation, cell migration, and cell proliferation are all performed through the effects of different cell responses and each response affects the way a tissue behaves (Lemmon and Weinberg, 2017). These ideas relate to the research question of how different subsets of FN (number of Fibronectin) molecules affect the different properties of a tissue.

Fibronectin is a multidomain glycoprotein that is part of the extracellular matrix (Schwarzbauer et al. 2011). Fibronectin molecules are able to bind to one another and to cell surface receptors, which aids in cellular mechanosensory operations (cell adhesion and cell migration). As an example, a fibronectin's stretched fiber's stress and strain rates can affect the mechanosensory proteins of the surrounding tissue, which can affect a disease's severity. The fibril assembly is the major part of the extracellular matrix that form linear and branched networks that connect neighboring cells (Singh et al 2013). Through microscopic and biochemical assays, binding sites have been discovered for fibronectin in which fibronectin dimers are formed through disulfide bonds and it was experimentally determined that the fibronectin matrix assembly is mediated by cells through integrin and cell binding domains (Ruoslathi and Obrink 1996). When the FN matrix is formed, it is was deemed that the FN is bound to a substrate through a tethering site which pulls on the FN, causing conformational changes to the FN as an actin filament pulls the FN away from the elastic substrate (Xu et al 2009). The fibronectin is attached

to the sliding actin filament through molecular clutches, integrin bonds between the fibronectin and the actin filament (Weinberg et al 2017). Due to the forces that pull and stretch the FN fibril, understanding these properties created due to the conformational changes of the FN fibril is important and how these properties are affected can help scientists understand the biological background of a diseases and the afflicted tissue.

Through computational methods via MATLAB, simulations of fibronectin assembly were performed with various, differing parameters. These parameters, Vu (the actin filament strand's velocity to stretch the FN) (nm/s) and Ksub (substrate stiffness of the elastic substrate attached to the FN molecule) (pN/nm), are altered to see how each value affects the different properties of the fibronectin. The properties that are reviewed are: stretched lengths, relaxed lengths, number of fibronectin molecules, force of substrate (Fsub), fraction of clutches, total amount of clutches, stretched to relaxed length ratio (SR Ratio), length to thickness ratio (LT Ratio), and focal adhesion size (FA), slope (force of the FN vs the stretched length of the FN), strain (the change in length of the stretched FN fiber per relaxed length of the fiber), stress (force exhibited by the stretched fibronectin fiber per unit of cross sectional area of the FN) rates of the stretched FN fibril from the actin filament, X (change in fibril stretch of relaxed and stretched), and fsub of fluctuating fibrils. These properties are important to review as they play an important role in tissue repair through cell attachment and cell migration and playing a part in the cases of integrin rupture repairs that occur to the FN matrix. By changing the parameters of actin velocity and substrate stiffness, it is possible to see how each property is affected as these parameters influence FN assembly. As an example, with high actin velocity the integrin bonds rupture, so how does having a high actin velocity change the properties of the FN?

With these simulations and the collected data, four mains questions will be answered. 1) Do the measurements at the end of fibril assembly, specifically fibril size (stretched length, relaxed length, the number of FN molecules, thickness) or fibril properties (stretched-to-relaxed length ratio, average clutch engagement, assembly time), depend on actin velocity or substrate stiffness? What are the distributions for these measures in terms of means, variance, and shape? 2) Do viscoelastic properties differ for different actin velocity or substrate stiffness with an example of slope of force vs displacement from rest. How do these properties differ while having different sub types of fibrils that are created during the assembly process? 3) For a given fibril size (e.g., fibril number or resting length), how much does the viscoelastic slope from rest differ? Does this depend on actin velocity or substrate stiffness? If there are differences, how can they be explained. 4) How do cells with different actin velocity (possibly on different substrates) respond to restretching of fibrils produced by cells with a different actin velocity (and possibly substrate) and with the number of myosin motors (NM)?

These four essential questions will be the basis of exploring how fibril assembly is affected by the changes in actin velocity and substrate stiffness. Simulations are conducted with various MATLAB files depending on which state of the fibronectin model is being observed (stretched, restretched, etc.). From there, values such as stretched lengths, relaxed lengths, slope, etc. will be measured and their means will be compared from one another based upon the different combinations of velocity and stiffness values. Pinpointing the difference between these various parameters and properties will help determine the molecular detail of fibronectin assembly.

Chapter 2a: Background

The biological process of Fibronectin Fibril Assembly is established at various phases such as embryogenesis and during wound healing process at the injured areas of the body (Clark et al, 1982). The Fibronectin (FN) is a protein that binds to the cell surface receptors, collagen, and other FN molecules and are assembled by cells into insoluble elastic fibrils (Schwarzbauer et al. 2011). These elastic fibrils play a crucial role in the process and functions of cell migration, cell adhesion, and the structural stability of the extracellular matrix. That is why this mechanism takes place during the wound healing process as the fibronectin not only acts as a blood clotting mechanism, but also as a tissue repairing mechanism, that helps create an insoluble fibril matrix at the site of injury (Mosher et al. 1991). Because of these various biological processes, FN and the FN assembly have been the subject of study for a multitude of research areas in terms of FN properties and Mechanotransduction.

Even though the mechanism of assembly of FN is known; however, it is still poorly understood (Lemmon and Weinberg, 2017). Extensive research has been performed on FN and FN assembly where properties such as force generation and mechanical responses have been tested. Much information was gathered in regard to the way FN is created and the way FN is bound to the Extracellular Matrix (ECM). When FN forms, the process of fibrillogenesis (the development of fibrils in connective tissue) controls what FN binds to and how the bonding is performed. The fibrillogenesis of FN utilizes cell generated forces that show FN-FN binding sites and that previous studies show there being multiple domains that contain these binding sites (Weinberg et al. 2017, Lemmon and Weinberg, 2017). These binding sites along with the FN-cell interactions may play a

key role in the process of wound healing as the FN-cell binding creates stability in the ECM whereas an interruption in these bindings can cause cell dispersal and a breakdown in the matrix (Schwarzbauer et al. 2011). In addition to these binding site interactions, the mechanical properties that the FN exhibit also play a vital role in disease progression.

Mechanical properties of the FN play an important to the severity of a disease. As an example, clinical trials have shown that tissue stiffness can cause the severity of the disease to increase as with patients with malignant tumors that have increased elastic modulus show more severe symptoms (Berg et al. 2015). From there, it has been established that the mechanically transduced signals determine cell fate and cellular function that inevitably affects diseases (Bangasser et al 2013). This mechanism is known as Mechanotransduction, which occurs by using transmembrane integrins that are linked by focal adhesion complexes. Myosin generated forces are created through these integrins and these forces act on the cytoskeleton to the surrounding extracellular substrate (Weinberg et al 2017). Forces such as stress, strain, etc. vary due to the interactions between the cell and the substrate surface. Because of these variable forces, cellular response can be altered and cellular responses to the substrate can be mediated or affected by the ECM (Weinberg et al. 2017). As an example, an *in vitro* FN model was created to imitate the wound healing process of the tissue. Tissue tension was observed across the gaps or wounds of the tissue where G-protein Rho signaling occurred due to the effects of the actin filament activity, extending fibronectin fibers into the wound gaps (Sakar et al 2016). It was observed that the rate of which cells migrated differed between treated tissues and non-treated tissues. ECM contains a variety of biological components and proteins in a tissue, such as FN, that are created during the stages of embryogenesis

and wound healing (Schwarzbauer et al 2011). Previous studies have shown that FN fibrils utilizes actomyosin forces in order to assemble and become elastic and extendable (Lemmon et al 2009). This assembly in depicted as a computational model, the Weinberg-Mair-Lemmon Model (**Figure 1**), that shows the actomyosin-FA-FN fibril substrate unit that simulates the assembly of a single FN fibril.

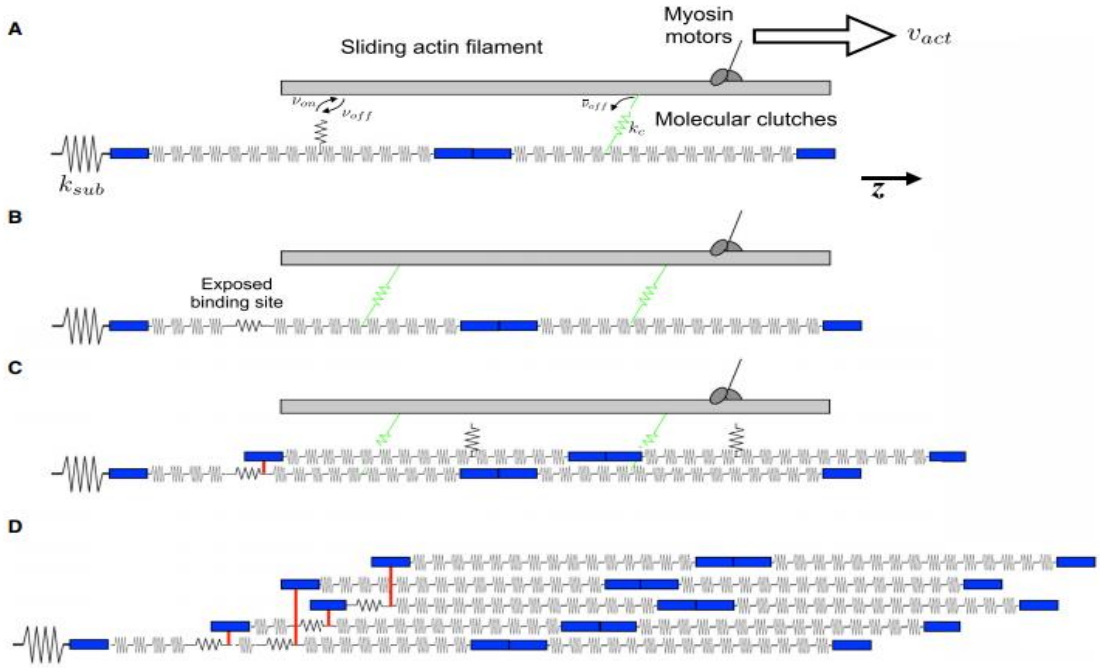

Figure 1: Schematic of the Weinberg-Mair-Lemmon FN model. (*A*) Assembly begins with a single FN molecule, represented by 30 springs in series, attached to an elastic substrate, with stiffness k_{sub}. Myosin motors pull on the sliding actin filament at velocity *Vu*. Molecular clutches reversibly bind the actin filament with rates v_{on} and v_{off}. Engaged molecular clutches transmit a force proportional to the clutch stiffness k_c and disengage with a force-dependent off-rate $\bar{v}_{off}$. Note that engaged clutches are connected in parallel with springs representing FN Type III domains. (*B*) Actomyosin-driven forces stretch the FN Type III domains, exposing a cryptic FN binding site. (*C*) A soluble FN molecule in the extracellular space binds to the exposed binding site. (*D*) Subsequent molecular clutch engagement, FN Type III domain stretching, and FN-FN binding events produce an elastic, insoluble FN fibril (Weinberg et al. 2017).

Figure 1 illustrates the Weinberg-Mair-Lemmon model of the FN assembly when cells bind to FN due to transmembrane integrins. The integrins, acting as molecular clutches, pass on actomyosin forces to the assembling FN fibril, indicating that FN fibrils only assemble due to contractile forces being exerted onto FN molecules (Lemmon et al

2009). The FN binding is performed through the exposure of a binding site and by having a soluble FN bind to the exposed binding site. The binding site is exposed as a stochastic process and it is modeled as such, with a probability of π^{j}_{i} predicted by a Hill equation with domain stretch equal to ϵ_t shown in **Equation 1** (Weinberg et al. 2017):

$$\pi_i^j = \frac{(\in_i^j)^n}{(\in_i^j)^n + \epsilon_t^n} \qquad \textbf{Equation 1}$$

Additionally, the model is simulated to show the FN assembly along a single dimension. When an FN molecule binds to the exposed binding site, the new FN molecule is placed to an open position, randomly, around the stretching FN molecule. Each FN molecule has six open positions for a new neighboring FN molecule to occupy and one all positions have been occupied, the FN molecule is rendered unable to bind to additional FN molecules. In order to reflect the mechanical properties of the model when the Type III domain is folded due to actin-myosin forces, a stretch-dependent stiffness relationship was created which would mimic a predicted stiffness as stretch increases. The steady-state stretch-dependent domain stiffness k_i^{∞} $(\in_i^j)$ transitions between unique stiffness and the Weinberg-Mair-Lemmon stiffness k_i^{∞}=ki,0 and for large $(\in_i^j)$, k_i^{∞} approaches $k_{\omega}(\in_i^j)$,

$$k_i^{\infty}\ (\in_i^j) = k_{\omega}(\in_i^j) + \left[k_{i,0} - k_{\omega}(0)\right]\exp(\frac{-\epsilon_i^j}{\lambda_{\omega}}) \qquad \textbf{Equation 2}$$

where λ_{ω} is a length scale that defines the transition; and k_{ω} is defined in **Equation 4**. For large domain stretches, the model relates the molecular force F_{ω} and elongation ϵ,

$$F_{\omega}(\epsilon) = \frac{k_B T}{X_p}\left[\frac{1}{4\left(1-\frac{\epsilon}{X_d}\right)^2} - \frac{1}{4} + \frac{\epsilon}{X_d}\right] \qquad \textbf{Equation 3}$$

where k_B is the Boltzmann's constant; T is the absolute temperature; χ_p is the domain persistence length; and χ_d is the domain contour length. To connect the model to the spring network, spring constant k_ω is defined by relating the force F_ω and displacement ϵ of spring from rest as the derivative of F_ω in **Equation 3,** in respective to ϵ,

$$k_\omega(\epsilon) = \frac{dF_\omega}{d\varepsilon} = \left(\frac{k_B T}{X_d X_p}\right)\left[\frac{1}{2\left(1-\frac{\epsilon}{X_d}\right)^3} + 1\right] \qquad \textbf{Equation 4}$$

To account for the changes of the transition between domain stiffnesses, the time-varying domain stiffness $k_i^j(t)$ is governed by a first-order isomerization reaction, with steady-state domain stiffness $k_i^\infty\left(\epsilon_i^j\right)$ and time constant τ_ω,

$$\frac{dk_i^j}{dt} = \left(\frac{k_i^\infty\left(\epsilon_i^j\right) - k_i^j}{\tau_\omega}\right) \qquad \textbf{Equation 5}$$

With these equations and mathematical approaches, the stretch and time dependent stiffness relationships are defined. This way, mechanical properties at rest can be defined and characteristic spring properties can be established, showing viscoelastic properties.

The Weinberg-Mair-Lemmon FN model shows a single FN that contains a series of Hookean springs that exhibits extensible domains of the FN and these springs are attached to an elastic substrate with a stiffness of k_{sub}. The FN model is presented as Hookean Springs due to the fact that the fibronectin fibers have a relaxed and a stretched position due to contractile forces. The actin filament shown is pulled across by myosin motors in with a velocity of V_{act}. The fibronectin assembly ends when the variable, V_{act}, reaches zero. Vu is the unloaded actin velocity where the maximum velocity can be reached for the actin fiber. Finally, Vu is the parameter where V_{act} is dependent upon as a variable as seen in **Equation 6** and being dependent upon the stall and traction forces.

$$V_{act} = V_u(1 - \frac{f_{sub}}{f_{stall}}) \qquad \textbf{Equation 6}$$

F_{stall} is the stall force dependent on the number of myosin motors and f_{sub} is the traction force that is determined by the spring constant, k_{sub} and the stretch, $\in$. The parameter of k_{sub} is connected to the series with the Hookean spring and together they represent the elasticity of the substrate. The "series" is stated to explain that the fibronectin model contains 29 independently folded domains where 15 Type III domains of the model can unfold in response to contractile forces (Weinberg et al 2017). The Vu is another important parameter that is a determining factor of the assembly process as when velocity reaches zero, the fibril assembly ends. Additionally, different cell types have varying values of actin velocities (Cuda et al. 1997). These two parameters, substrate stiffness and actin velocity, are both crucial factors in the FN assembly. Therefore, it is under speculation that these parameters may also play a key role as determining factors for FN properties (Weinberg et al. 2017).

With the clarity that the substrate stiffness and actin velocity are important factors in FN assembly, it has been theorized that these two parameters may also play key roles determining the mechanical properties of the FN fibril. A computational simulation of a single FN assembly was performed with the properties of stretched lengths, relaxed lengths, thickness, substrate force, etc. have been recorded (**Figure 2**) (Weinberg et al 2017). This time series measurement of a single simulation shows that the fibril lengths, stretched length and relaxed length, as well as with other important properties of the FN fibril to increase with an increase in time. It was noted that with an increase in the substrate force, the actin velocity decreases, and it has been known that an increase in actin velocity is known to stop the fibril assembly process due to integrin binding ruptures

(Bangasser et al 2013). In order to procure further insight on these properties, histograms of the FN fibril measurements were collected with having 500 simulations being performed (**Figure 3**) (Weinberg et al 2017). These simulations showed that the substrate force, and relaxed and stretched length of the assembled FN fibril are positively correlated with the FA (Focal Adhesion) length, and independent of substrate stiffness. Furthermore, experiments were conducted in order to investigate the substrate stiffness dependency of the relationship between FA length and the fibril properties (Weinberg et al 2017) (Fu et al. 2010). It has been shown that the substrate stiffness increases the FA stress and FN fibril length-FA length ratio ratios increase with an increase in substrate stiffness rigidity. In doing so, these simulations and histograms show that the actin velocity, Vu, and substrate stiffness, k_{sub}, play key roles in the property shaping step of the FN fibril.

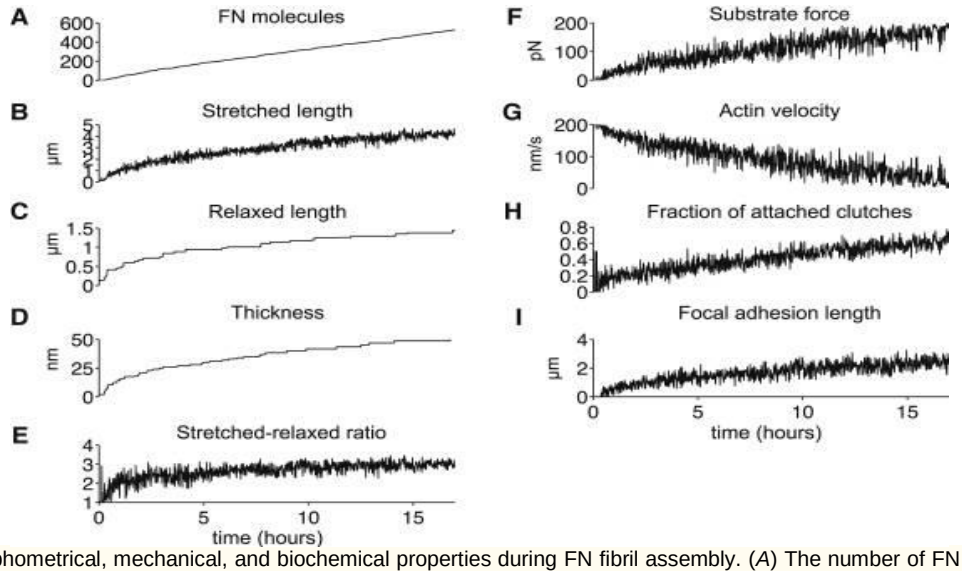

Figure 2: Morphometrical, mechanical, and biochemical properties during FN fibril assembly. (*A*) The number of FN molecules, (*B*) stretched length, (*C*) relaxed length, (*D*) thickness, (*E*) extensibility, given by the stretched-relaxed length ratio, (*F*) substrate force, (*G*) actin filament velocity, (*H*) the fraction of attached molecular clutches, and (*I*) the FA length are shown as a function of time for a 16-h simulation of an assembling FN fibril. The fraction of attached molecular clutches is given by total clutches bound to the FN Type III-10 domain, divided by the total number of clutches available for binding (two per exterior FN molecule). (Weinberg et al 2017).

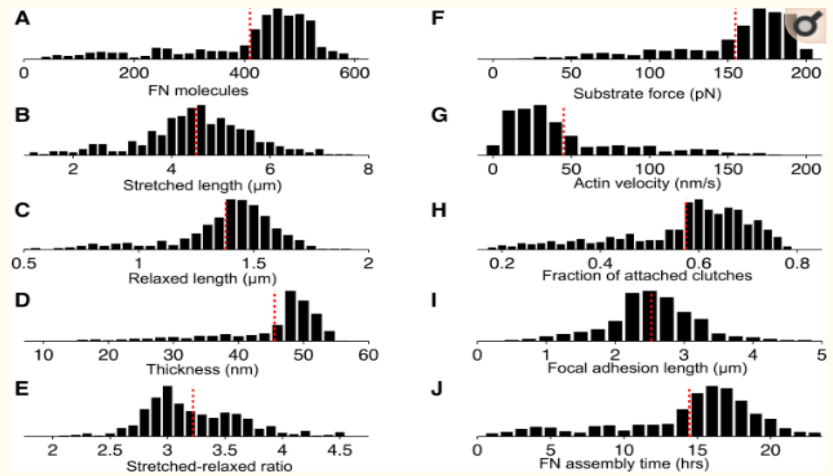

Figure 3: Summary of morphometrical, mechanical, and biochemical properties of assembled FN fibrils. Histograms for the following measurements and properties are shown for 500 numerical simulations: (*A*) number of FN molecules, (*B*) stretched length, (*C*) relaxed length, (*D*) thickness, (*E*) extensibility, given by the stretched-relaxed length ratio, (*F*) substrate force, (*G*) actin filament velocity, (*H*) the fraction of attached molecular clutches, and (*I*) FA length. (*J*) Summary data for total assembly time is shown. In all panels, the dashed red line denotes the mean. (Weinberg et al 2017).

Previous studies have shown that the parameter, substrate stiffness - k_{sub}, plays a key role in the FN assembly and it has also been documented that Vu can affect the assembly process of the FN as well (Weinberg et al 2017). Due to these reasons, it has now become important to understand how these parameters can affect the various fibril and mechanical properties of the FN at the same time. In order to see the relationships between the two parameters and the major FN properties, computational experiments and modelling were conducted. Properties such as: stretched lengths, relaxed lengths, number of fibronectin molecules, force of substrate (Fsub), fraction of clutches (number of integrin bonds between the actin filament and the FN molecule [two bonds per FN]), total amount of clutches, stretched to relaxed ratio (SR Ratio), length to thickness ratio (LT Ratio), focal adhesion (FA), slope, stress, strain, etc. were tested with the two parameters at differing values. Using computational modelling, simulations were performed to obtain FN assemblies with differing substrate stiffnesses as well as differing

acting velocities. Each substrate stiffness was paired with each actin velocity until each fibril assembly had a unique k_{sub}-Vu (actin velocity for the simulation) pairing. Each assembly was performed for 100 simulations over time and the data was compiled and analyzed through the programming software, MATLAB. Each assembly's property was analyzed, and additional assemblies were performed in order to compare the differences between stretched fibrils and re-stretched fibrils properties. Collected data will be presented in the form of diagrams in order to see differences of values for a given property against each k_{sub}-Vu pairing. Visual representation of the data will be the main factor in determining how each property changes depending upon the given k_{sub}-Vu pairing.

In addition to the k_{sub}-Vu pairing, one last analysis was performed with an additional parameter, NM (the number of myosin motors). As shown in **Figure 1**, myosin motors pull on the actin filament with a velocity of V_{act}. This parameter is important to note as the number of myosin motors may have an effect on the elongation of the fibronectin fibers which may affect the substrate stiffness as mentioned by Weinberg and his team (Weinberg et al 2017). From **Equation 6**, it was determined that the number of myosin motors affect the stall force of the fibronectin assembly; meaning that NM has the ability terminate the fibronectin assembly. Due to these reasons, NM is another important parameter to be experimented alongside k_{sub} and Vu. Through these simulations and analysis, insight will be procured on how these three major parameters affect the way FN assembly is performed and will also give clarity on whether one of these parameters has a greater effect on FN properties than the other.

In order to understand the viscoelastic properties of the fibril matrix, an additional set of simulations were performed and analyzed. Assembled fibrils were relaxed by

removing integrin attachments and then “re-stretched” by conducting cell re-attachment. This “Restretched Model” was created to replicate the moment where an assembled fibril remains after a cell migrates away from the site of assembly and the fibril left behind is then restretched by another cell. In response, two unique fibril sub types were observed due to the restretching labeled “stably stretched fibril” (SSF) and “fluctuating stretched fibril” (FSF). SSFs are fibrils that show constant force and stretch without restretching whereas FSFs are fibrils that show fluctuations with time in force and stretch due to restretching. Their differences are shown in **Figure 4** with SSF (red) and FSF (blue).

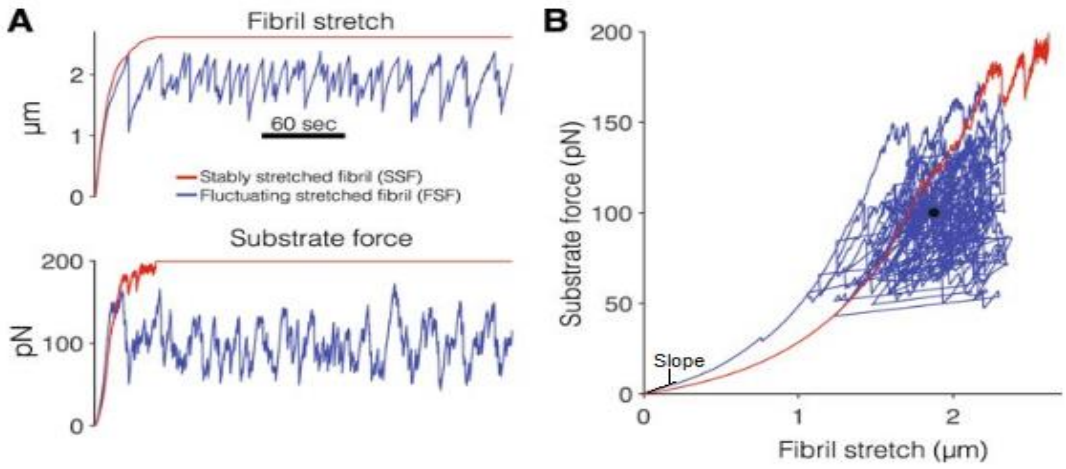

Figure 4: The differences between the two subtypes of viscoelastic fibrils. (A) The fibril stretch (difference between the stretched length and relaxed length) and substrate force are shown as a function of time with SSF in red and FSF in blue. (B) Substrate force is shown as a function of fibril stretch for the representative SSF and FSF. Solid black circle represents the mean substrate force and fibril stretch for FSF during the final two minutes of the simulation time. The slope of the fibril is highlighted in black to illustrate the point where the slope is determined for the fibril (Lemmon and Weinberg, 2017).

These fibril subtypes are important to compare and contrast as these subtypes show a difference in terms of viscoelastic properties (force, stretch, slope, etc.). Therefore, it is fundamental to understand how k_{sub} and Vu are able to alter these properties. Understanding these differences between these subtypes could play a significant role in the mechanics of the provisional extracellular matrix (Lemmon and Weinberg 2017).

Chapter 2b: Modelling and Simulations

A computational FN fibril assembly model and the cell-FN fibril substrate interactions were created by the Lemmon-Weinberg group based on the Chan-Odde model. This model contains the FNIII domain with Hookean springs (Figure 1) that is designed to be elastic and stretchable. There are 30 FNIII domains in each FN dimer and FN-FN bindings occur during assembly. FN fibrils exhibit actomyosin forces due to the integrin bindings between the cell surface and the fibril and these forces stretch individual FNIII domains which allows the binding of new FN molecules. Each new integrin binding occurs with the addition of new FN molecules, which creates an insoluble elastic FN fibril (Weinberg et al 2017).

With this model, three steps occur for the FN assembly: initialization, iteration, and termination. The initiation step illustrates the initial conditions for the simulation of having domain displacements, clutch displacements, clutch state, stiffness, nFN (number of fibronectin molecules in the assembly), exponential random variables, global time, network connections, and spring network. The nFN starts off with a value of 1 and is bound to the substrate.

Next, the Iteration phase where the second molecule binds itself to the first molecule, and the third molecule connects to the second, and so forth. All FN molecules after the first FN molecule have FN-FN binding. Afterwards, the FNIII domain node displacement occurs and molecular clutch engagement/disengagement takes place. Each FN molecule has two clutch binding sites and a global time step will point out when this binding reaction will occur. Once it is known on how long the reaction occurs, the time it takes for the next reaction is calculated. A clutch engagement/disengagement are

stochastic chemical reactions where the binding reaction happens randomly for a FN molecule. From there, computational equations are used to decide if the local time steps do not exceed the global time step and if a reaction will occur in this global time step. The next step is the clutch node displacement, which are updated based on the actin velocity.

At the addition point of the FN molecules, domain stiffness is updated, and the FN-FN binding is defined based on whether the domain is bound to a FN molecule or not. From there, a connection between the domain and the new FN molecule is added to the growing fibril and the following sets of parameters are updated: if the domain is occupied, then the nFN increases, which resets the clutch and updates the stiffness of the fibril. The architecture of the fibril and the global stiffness of the dimer are updated, and the global time step of the assembly process is checked and updated. Finally, the termination phase occurs when the global time step equals the total time of assemblage, or if the actin velocity reaches a certain threshold (0.005 Vu). This actin velocity value is the point where actomyosin forces begin to stall (Weinberg et al 2017).

With this data assemblage, experimentation can be performed by varying the different parameters and properties of the fibrils. Naturally occurring ranges for actin velocity are between 10-5000 nm/s and naturally occurring ranges for substrate stiffness are between 0.1-500 pN/nm (Chan and Odde, 2008)(Cuda et al 1997). For these experiments, an actin velocity range of 10-10000 nm/s and substrate stiffness range of 0.1-1000 pN/nm will be used.

Chapter 3a: Results for Experiment 1

The first set of experiments were conducted in order to answer question 1. Do the measurements at the end of fibril assembly, specifically fibril size (stretched length, relaxed length, the number of FN molecules, thickness) or fibril properties (stretched-to-relaxed length ratio, average clutch engagement), depend on actin velocity or substrate stiffness? What are the distributions for these measures in terms of means, variance, and shape? To answer this, a dataset containing the resulting values of the viscoelastic properties of the varying fibril assembly simulations was collected in the form of .mat files.

The fibril assembly simulations were based off of the Weinberg-Mair-Lemmon model with varying parameters of k_{sub} and Vu. Each simulation had a unique k_{sub}-Vu pairing with a k_{sub} range of: [0.1, 0.3, 1, 3, 10, 30, 100, 300, 1000], and with a Vu range of: [10, 30, 100, 300, 1000, 3000 10000]. Altogether, there were 63 fibril assembly simulations that were performed via MATLAB with a unique k_{sub}-Vu pairing. Each unique parameter pairing assembly was performed again until 100 assembly simulations were created in order to reduce and possible assembly errors. Each assembly was performed and completed in 24 hours and values for each significant property was collected every 60 seconds. Through MATLAB, the average values for each property was calculated by averaging the specific property values from the 100 simulations of a unique parameter pairing. The averages were illustrated in histograms with each histogram showing the unique parameter pairing values as shown in **Figures 5A-19A**. The average value for a specific parameter pairing is shown with a red vertical line. **Figures 5B-19B** depict line graphs where a parameter is plotted against the unique property's mean value.

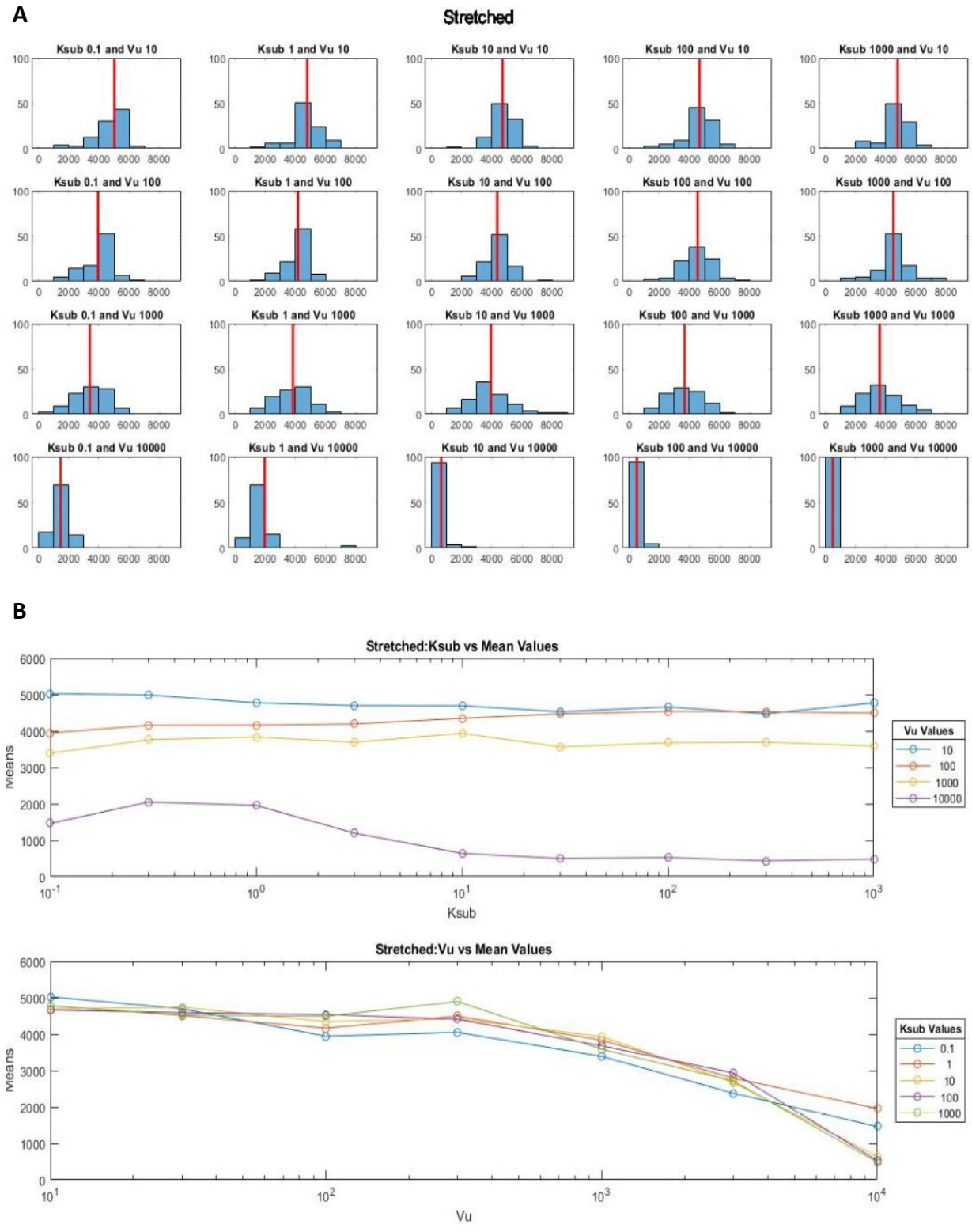

Figure 5: Results for the stretched length (nm) of the fibril assembly. (A) Histograms showing the varying values for each unique k_{sub}-Vu pairing. Parameter k_{sub} of [0.1, 1, 10, 100, 1000] and parameter Vu of [10, 100, 1000, 10000] were shown to observe jump in values. Red line is the mean for all simulations. (B) Line graphs showing each parameter versus the differing mean values (nm) for the property.

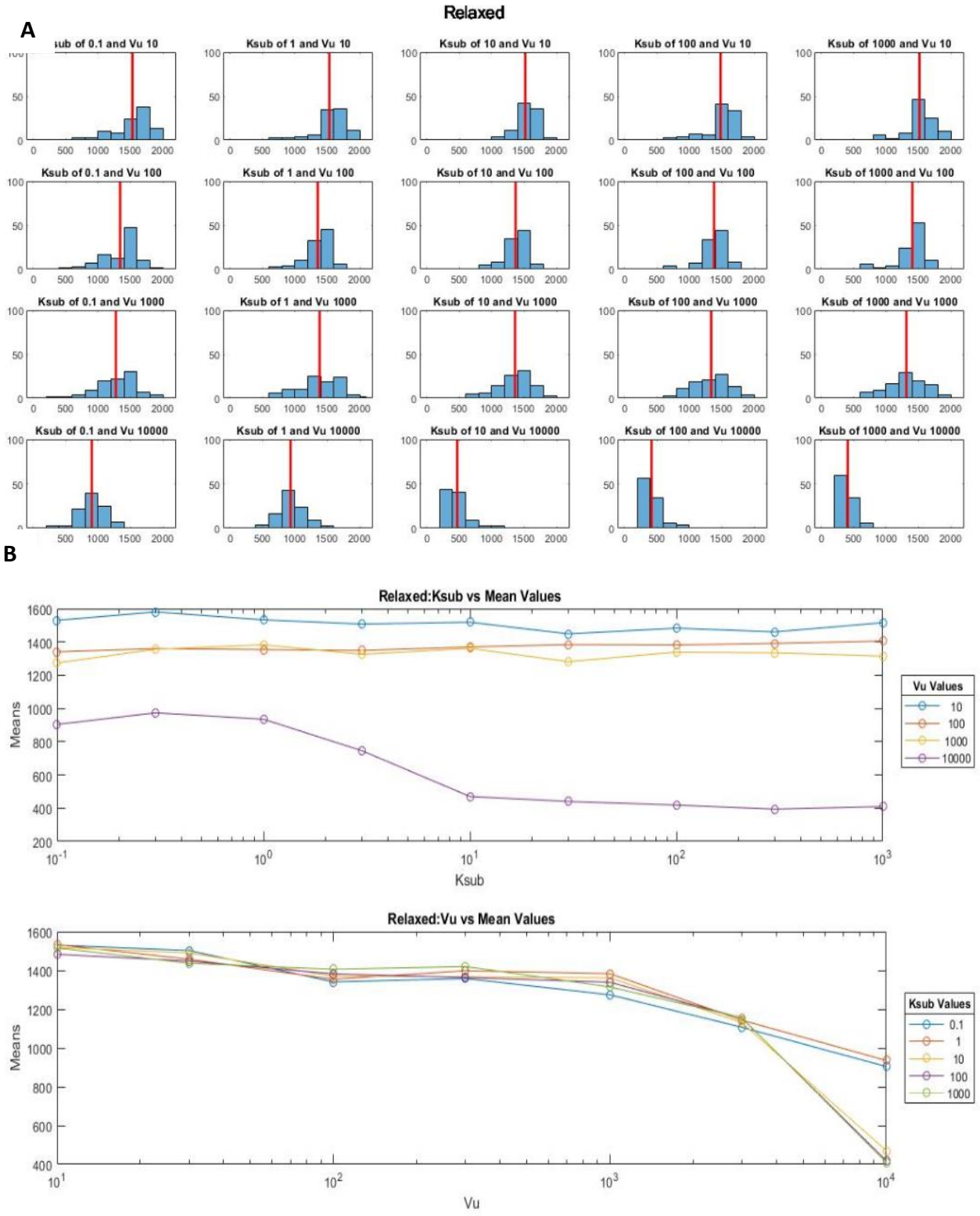

Figure 6: Results for the relaxed length (nm) of the fibril assembly. (A) Histograms showing the varying values for each unique k_{sub}-Vu pairing. Parameter k_{sub} of [0.1, 1, 10, 100, 1000] and parameter Vu of [10, 100, 1000, 10000] were shown to observe jump in values. Red line is the mean for all simulations. (B) Line graphs showing each parameter versus the differing mean values (nm) for the property.

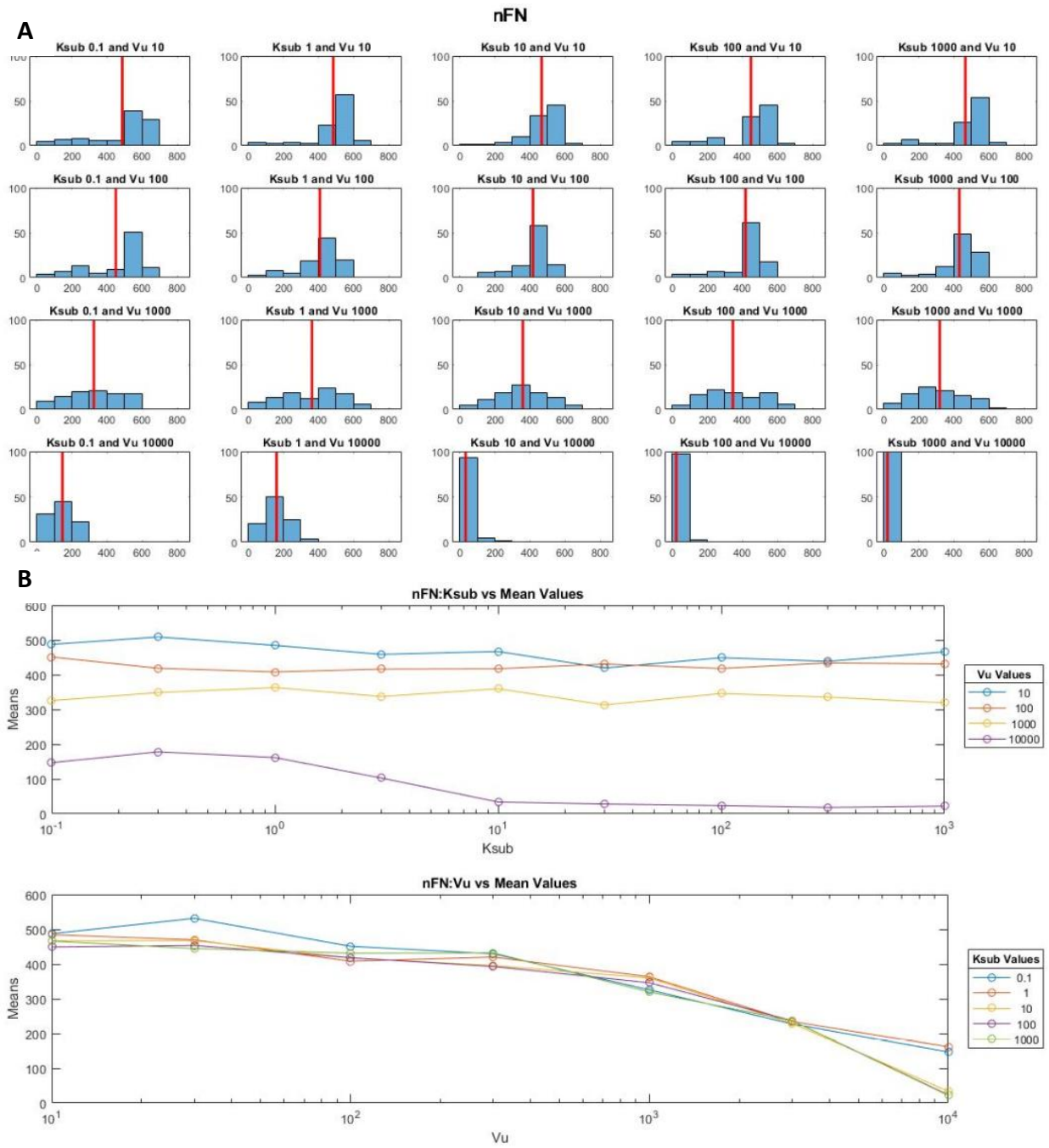

Figure 7: Results for the nFN of the fibril assembly. (A) Histograms showing the varying values for each unique k_{sub}-Vu pairing. Parameter k_{sub} of [0.1, 1, 10, 100, 1000] and parameter Vu of [10, 100, 1000, 10000] were shown to observe jump in values. Red line is the mean for all simulations. (B) Line graphs showing each parameter versus the differing mean values for the property.

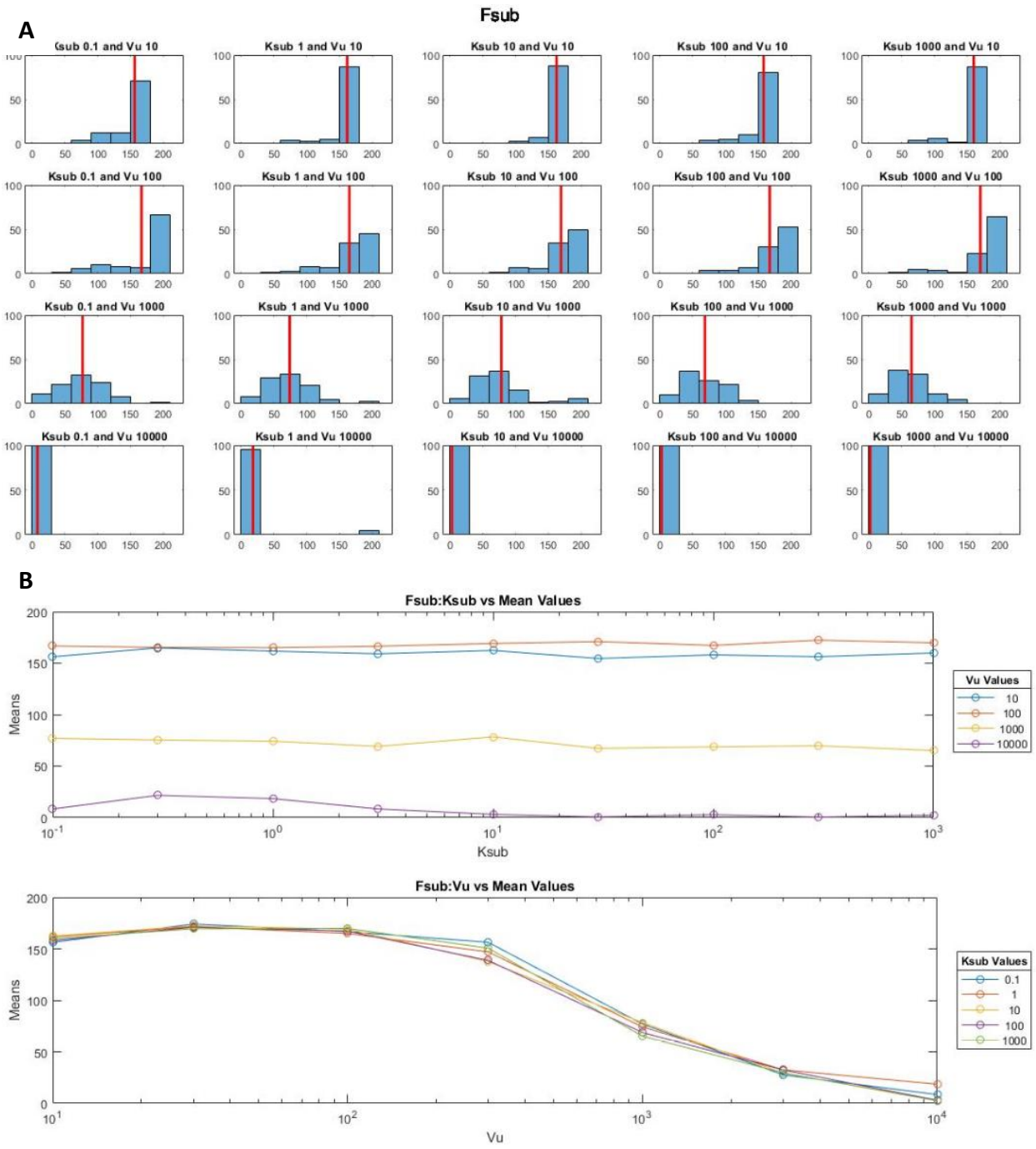

Figure 8: Results for the fsub (pN) of the fibril assembly. (A) Histograms showing the varying values for each unique k_{sub}-Vu pairing. Parameter k_{sub} of [0.1, 1, 10, 100, 1000] and parameter Vu of [10, 100, 1000, 10000] were shown to observe jump in values. Red line is the mean for all simulations. (B) Line graphs showing each parameter versus the differing mean values (pN) for the property.

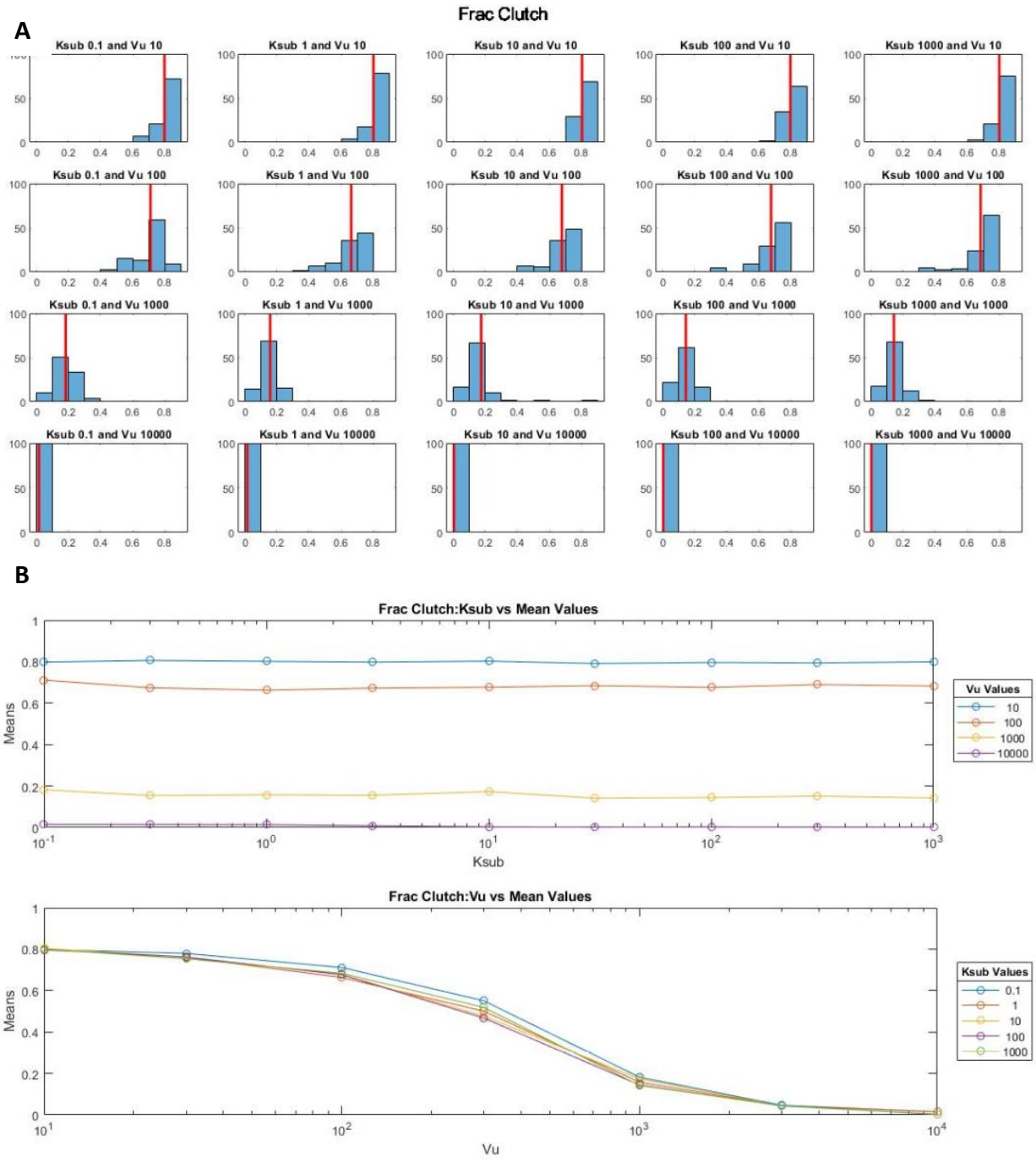

Figure 9: Results for the frac clutch of the fibril assembly. (A) Histograms showing the varying values for each unique k_{sub}-Vu pairing. Parameter k_{sub} of [0.1, 1, 10, 100, 1000] and parameter Vu of [10, 100, 1000, 10000] were shown to observe jump in values. Red line is the mean for all simulations. (B) Line graphs showing each parameter versus the differing mean values for the property.

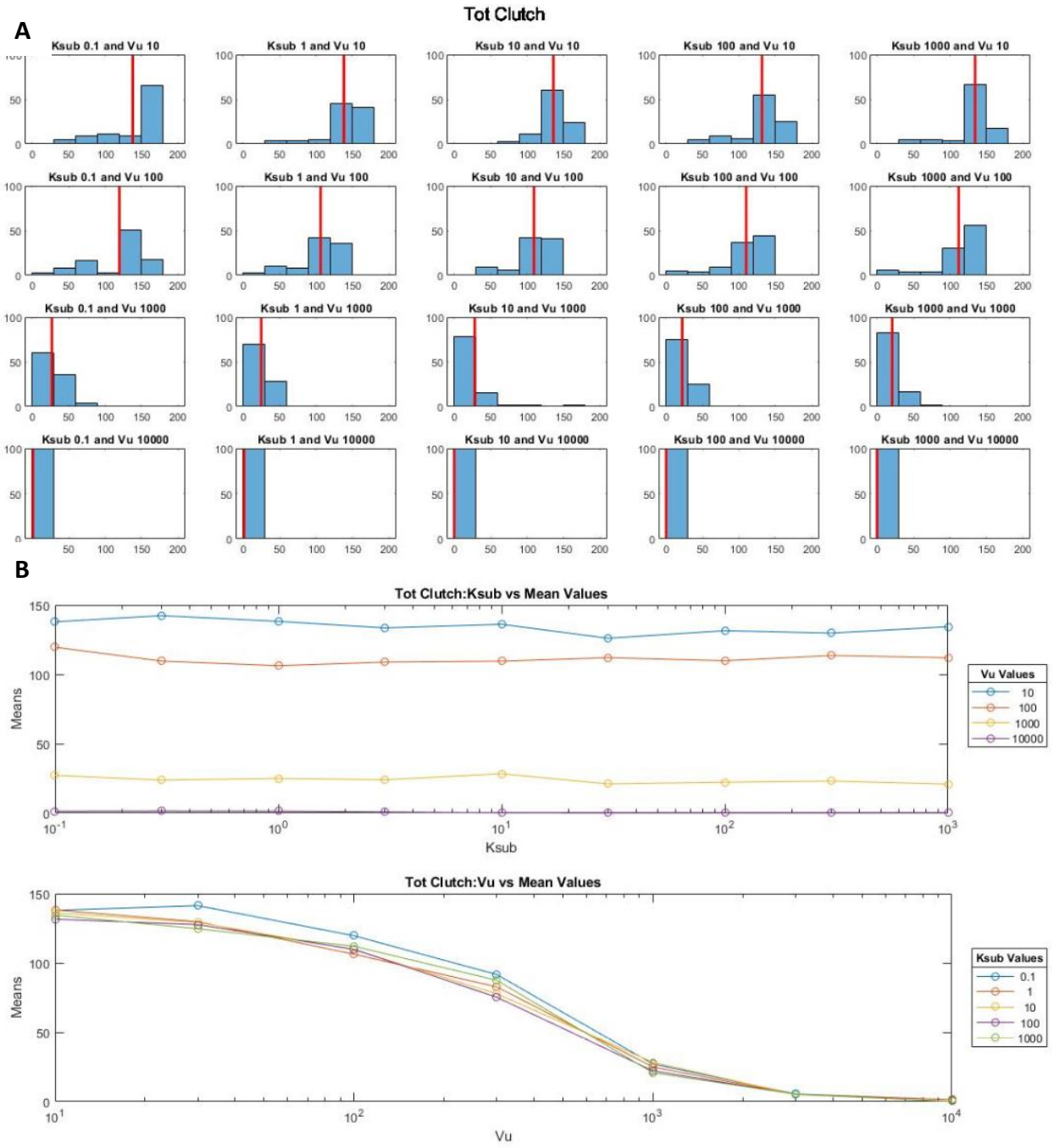

Figure 10: Results for the tot clutch of the fibril assembly. (A) Histograms showing the varying values for each unique k_{sub}-Vu pairing. Parameter k_{sub} of [0.1, 1, 10, 100, 1000] and parameter Vu of [10, 100, 1000, 10000] were shown to observe jump in values. Red line is the mean for all simulations. (B) Line graphs showing each parameter versus the differing mean values for the property.

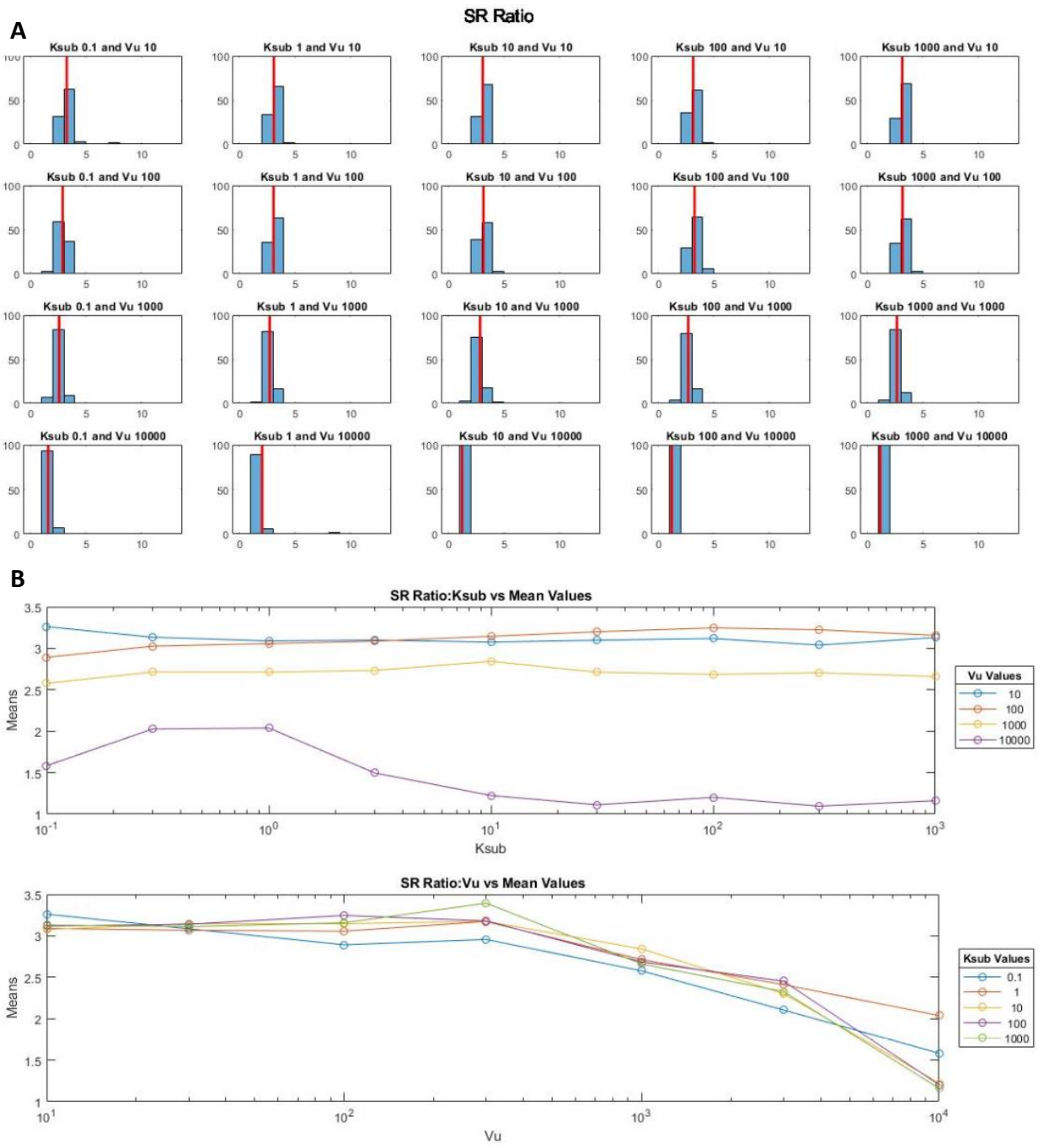

Figure 11: Results for the SR Ratio of the fibril assembly. (A) Histograms showing the varying values for each unique k_{sub}-Vu pairing. Parameter k_{sub} of [0.1, 1, 10, 100, 1000] and parameter Vu of [10, 100, 1000, 10000] were shown to observe jump in values. Red line is the mean for all simulations. (B) Line graphs showing each parameter versus the differing mean values for the property.

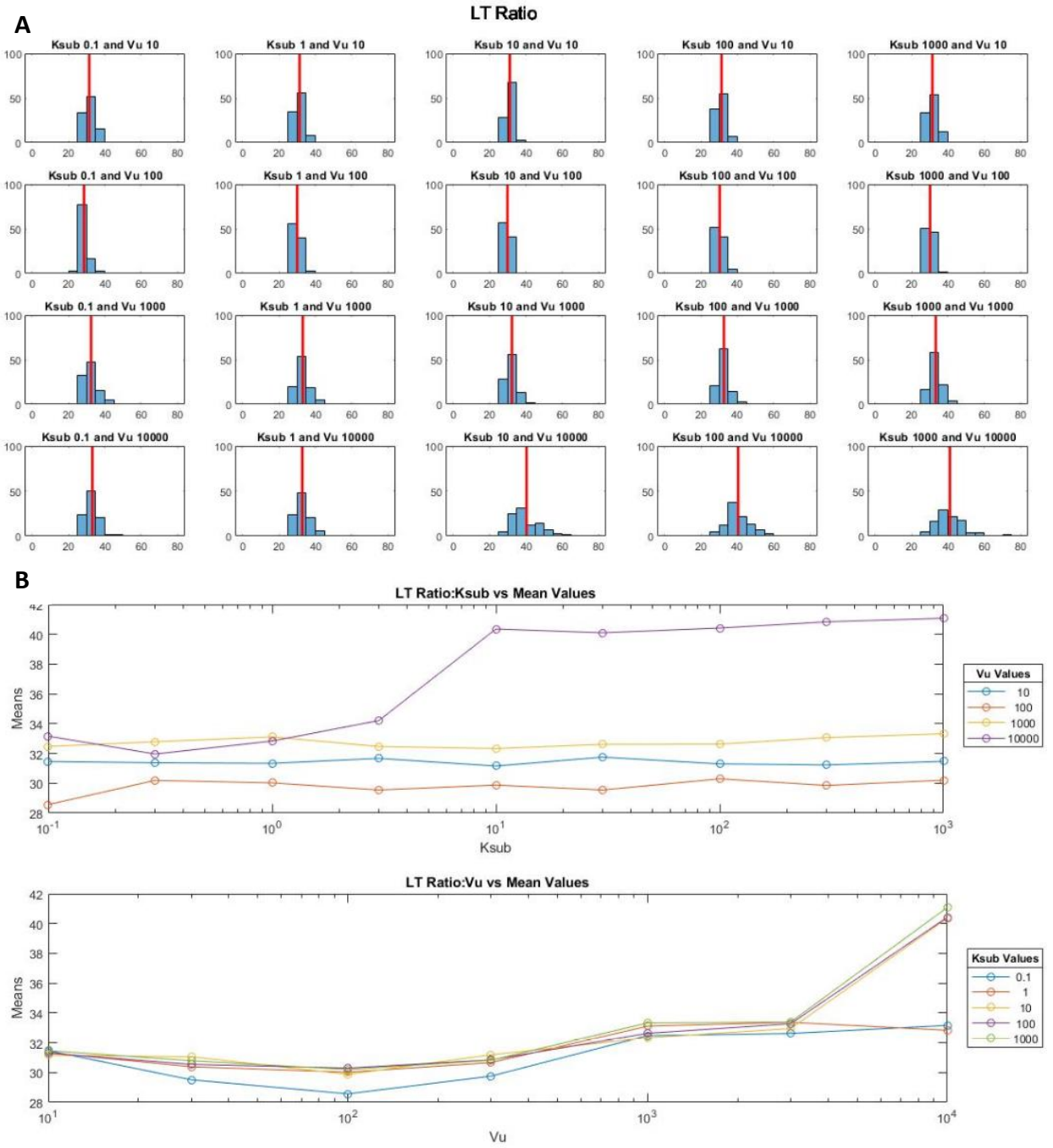

Figure 12: Results for the LT Ratio of the fibril assembly. (A) Histograms showing the varying values for each unique k_{sub}-Vu pairing. Parameter k_{sub} of [0.1, 1, 10, 100, 1000] and parameter Vu of [10, 100, 1000, 10000] were shown to observe jump in values. Red line is the mean for all simulations. (B) Line graphs showing each parameter versus the differing mean values for the property.

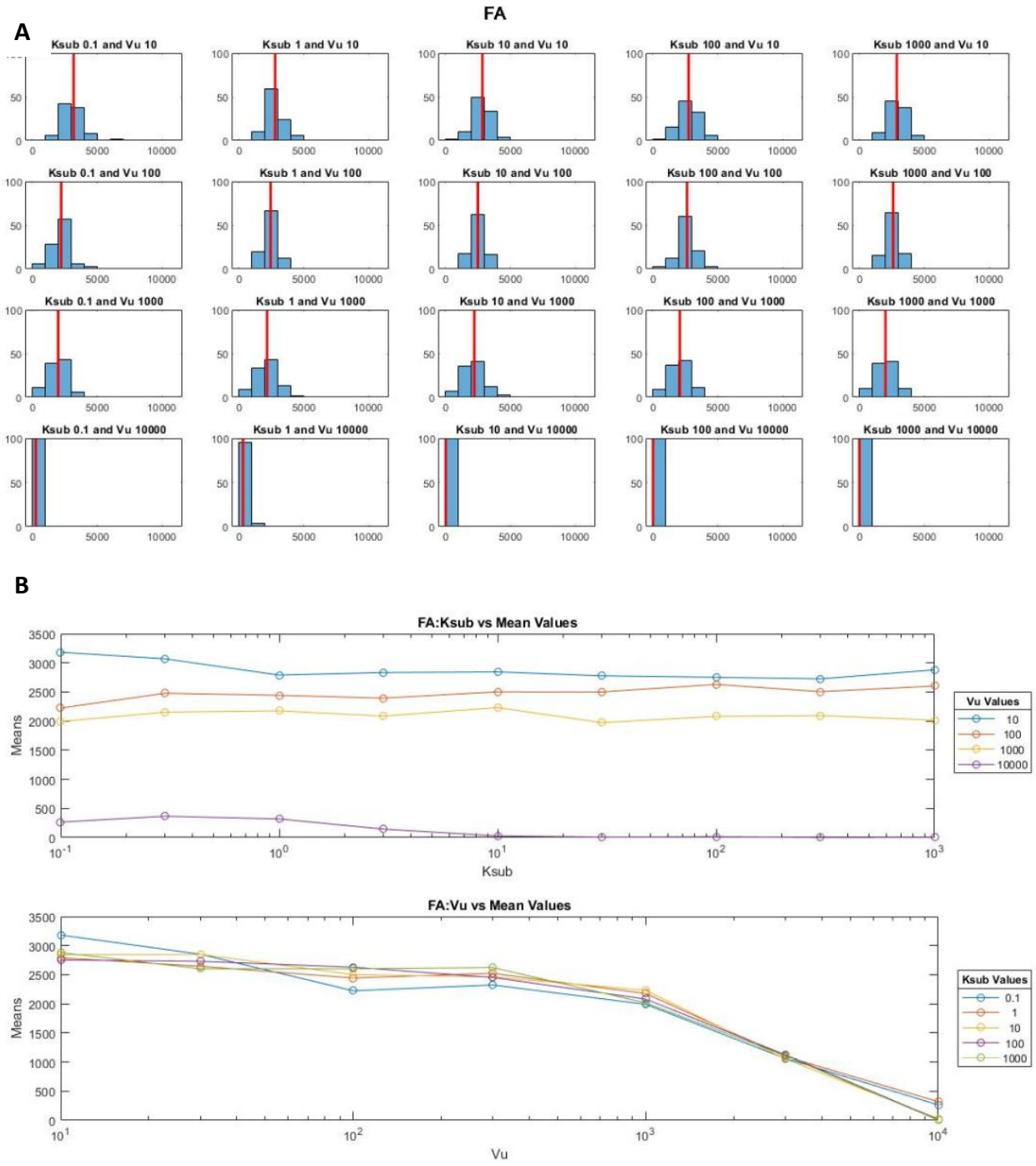

Figure 13: Results for the focal adhesion of the fibril assembly. (A) Histograms showing the varying values for each unique k_{sub}-Vu pairing. Parameter k_{sub} of [0.1, 1, 10, 100, 1000] and parameter Vu of [10, 100, 1000, 10000] were shown to observe jump in values. Red line is the mean for all simulations. (B) Line graphs showing each parameter versus the differing mean values for the property.

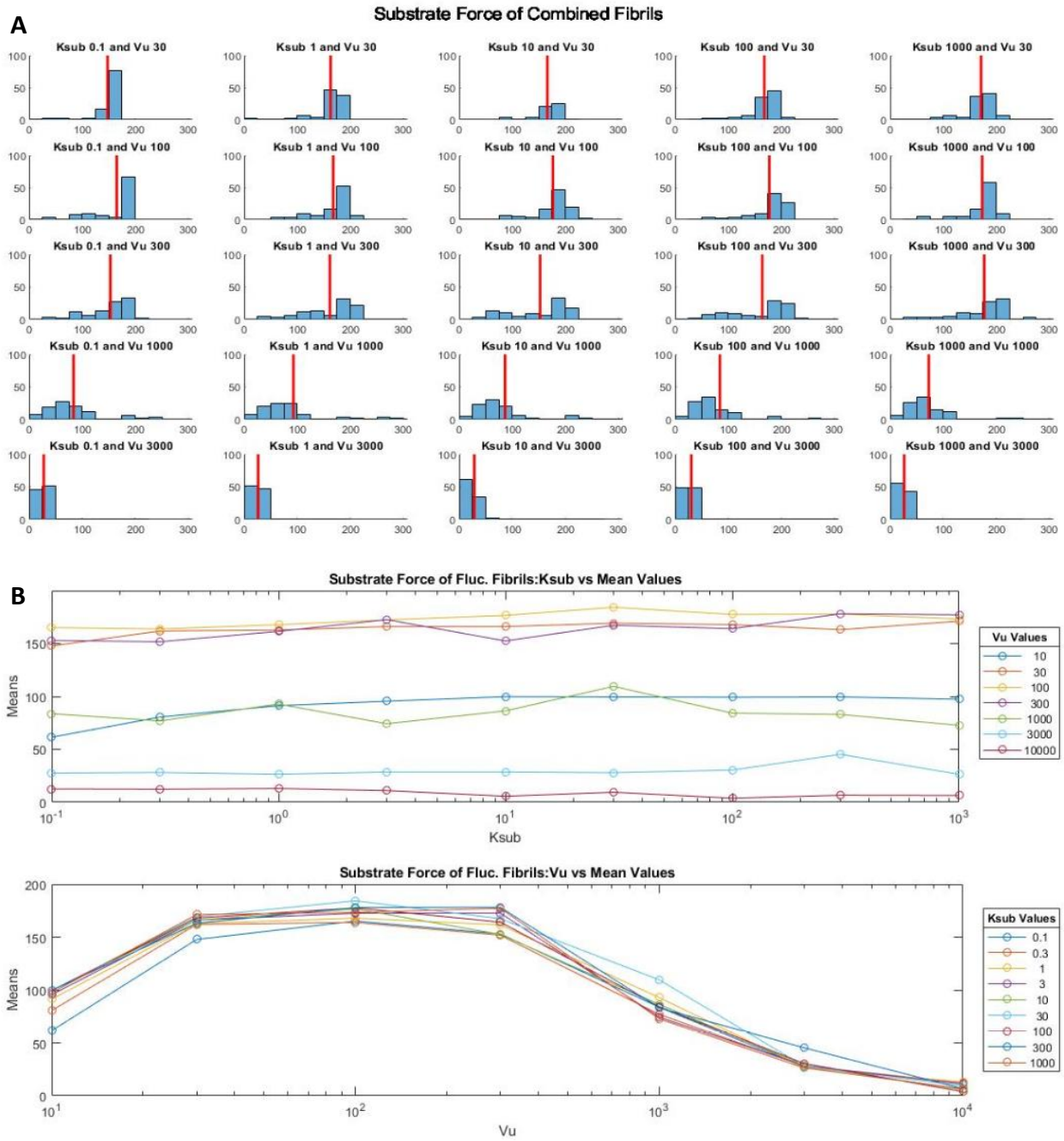

Figure 14: Results for the substrate force (pN) for SFs. (A) Histograms showing the varying values for each unique k_{sub}-Vu pairing. Parameter k_{sub} of [0.1, 1, 10, 100, 1000] and parameter Vu of [30, 100, 300, 1000, 3000] were shown to observe jump in values. Red line is the mean for all simulations. (B) Line graphs showing each parameter versus the differing mean values (pN) for the property.

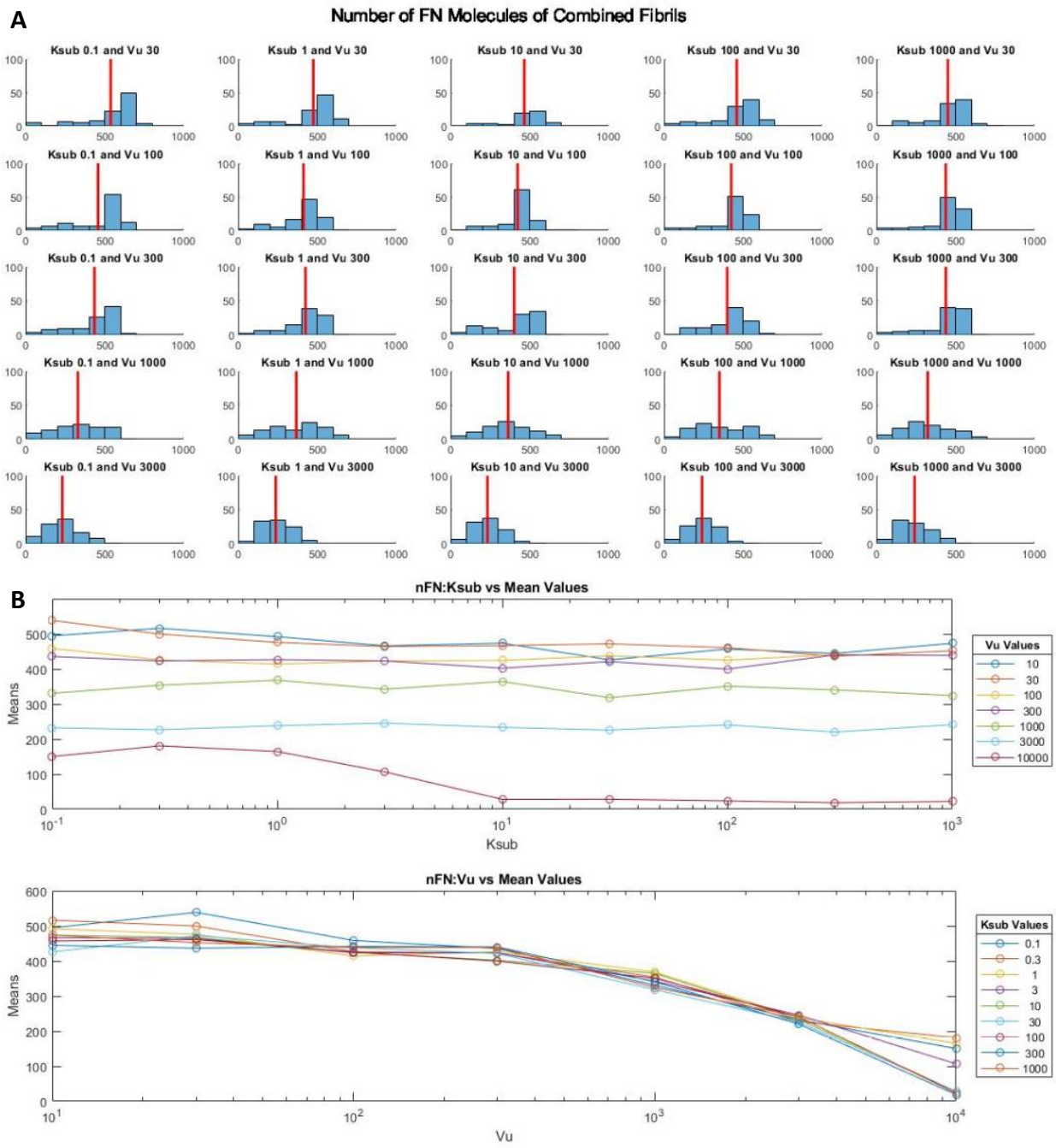

Figure 15: Results for the nFN for SFs. (A) Histograms showing the varying values for each unique k_{sub}-Vu pairing. Parameter k_{sub} of [0.1, 1, 10, 100, 1000] and parameter Vu of [30, 100, 300, 1000, 3000] were shown to observe jump in values. Red line is the mean for all simulations. (B) Line graphs showing each parameter versus the differing mean values for the property.

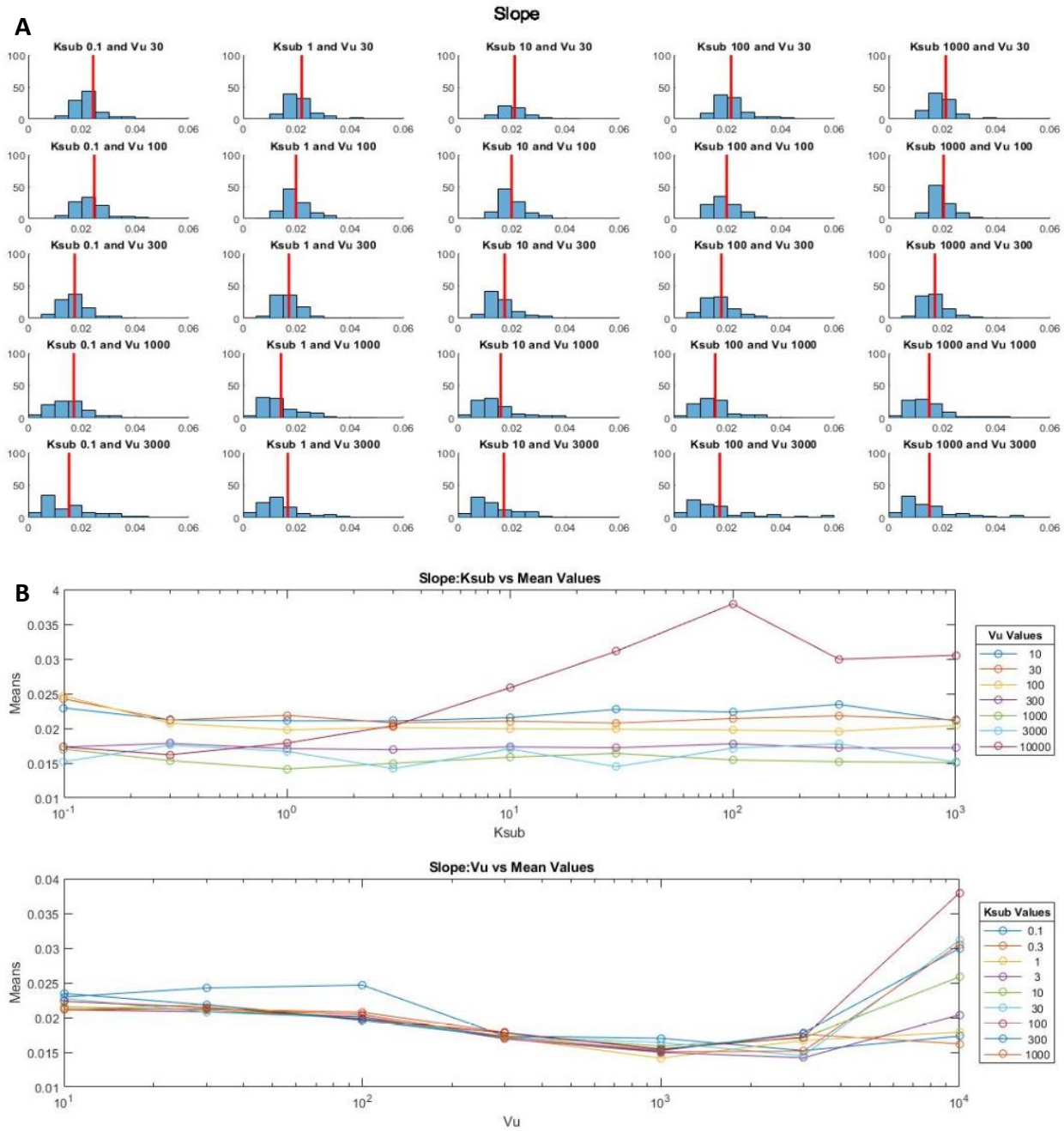

Figure 16: Results for the slope (pN/nm) for SFs. (A) Histograms showing the varying values for each unique k_{sub}-Vu pairing. Parameter k_{sub} of [0.1, 1, 10, 100, 1000] and parameter Vu of [30, 100, 300, 1000, 3000] were shown to observe jump in values. Red line is the mean for all simulations. (B) Line graphs showing each parameter versus the differing mean values for the property.

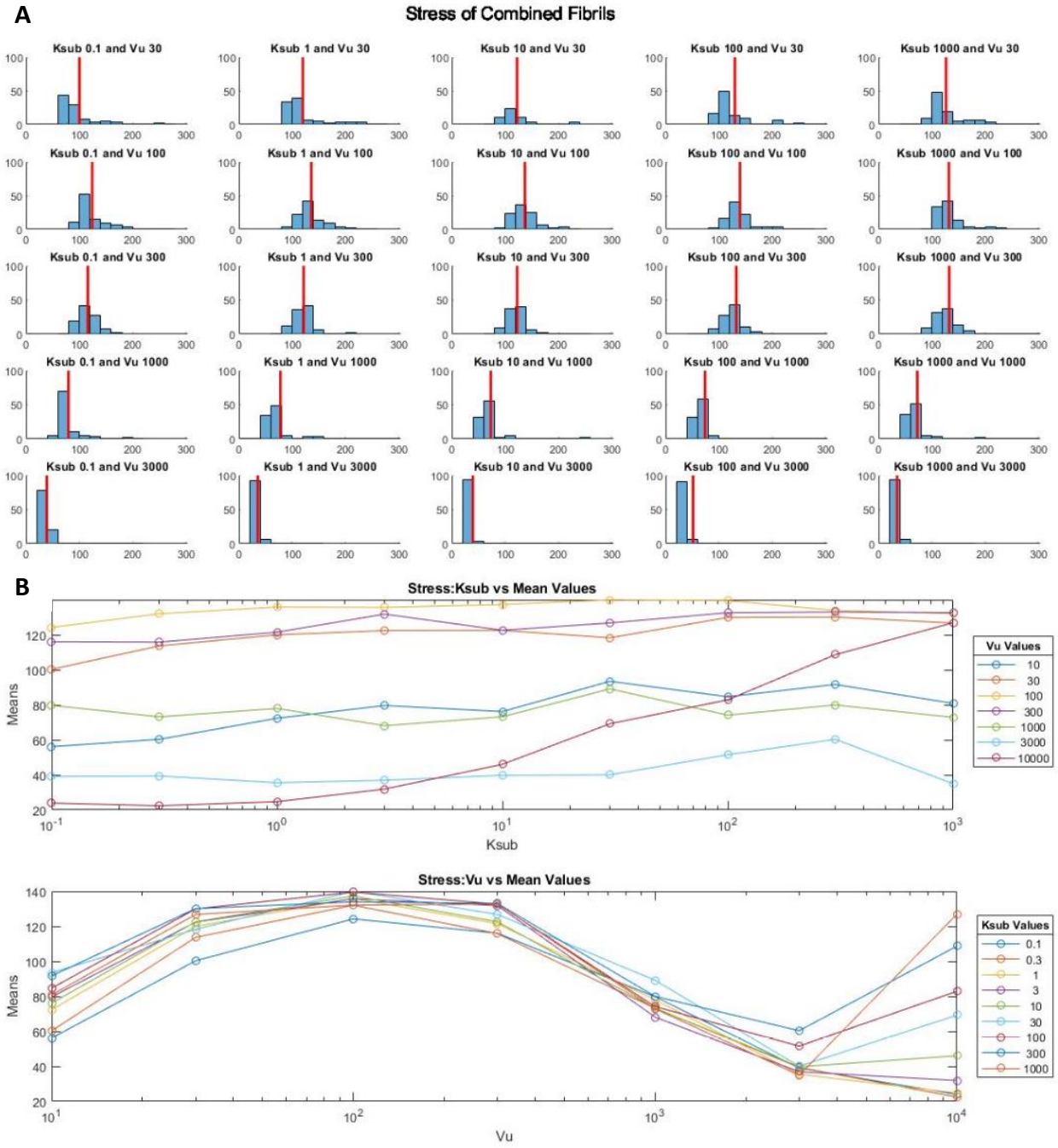

Figure 17: Results for the stress (pN per nm^2) for SFs. (A) Histograms showing the varying values for each unique k_{sub}-Vu pairing. Parameter k_{sub} of [0.1, 1, 10, 100, 1000] and parameter Vu of [30, 100, 300, 1000, 3000] were shown to observe jump in values. Red line is the mean for all simulations. (B) Line graphs showing each parameter versus the differing mean values for the property.

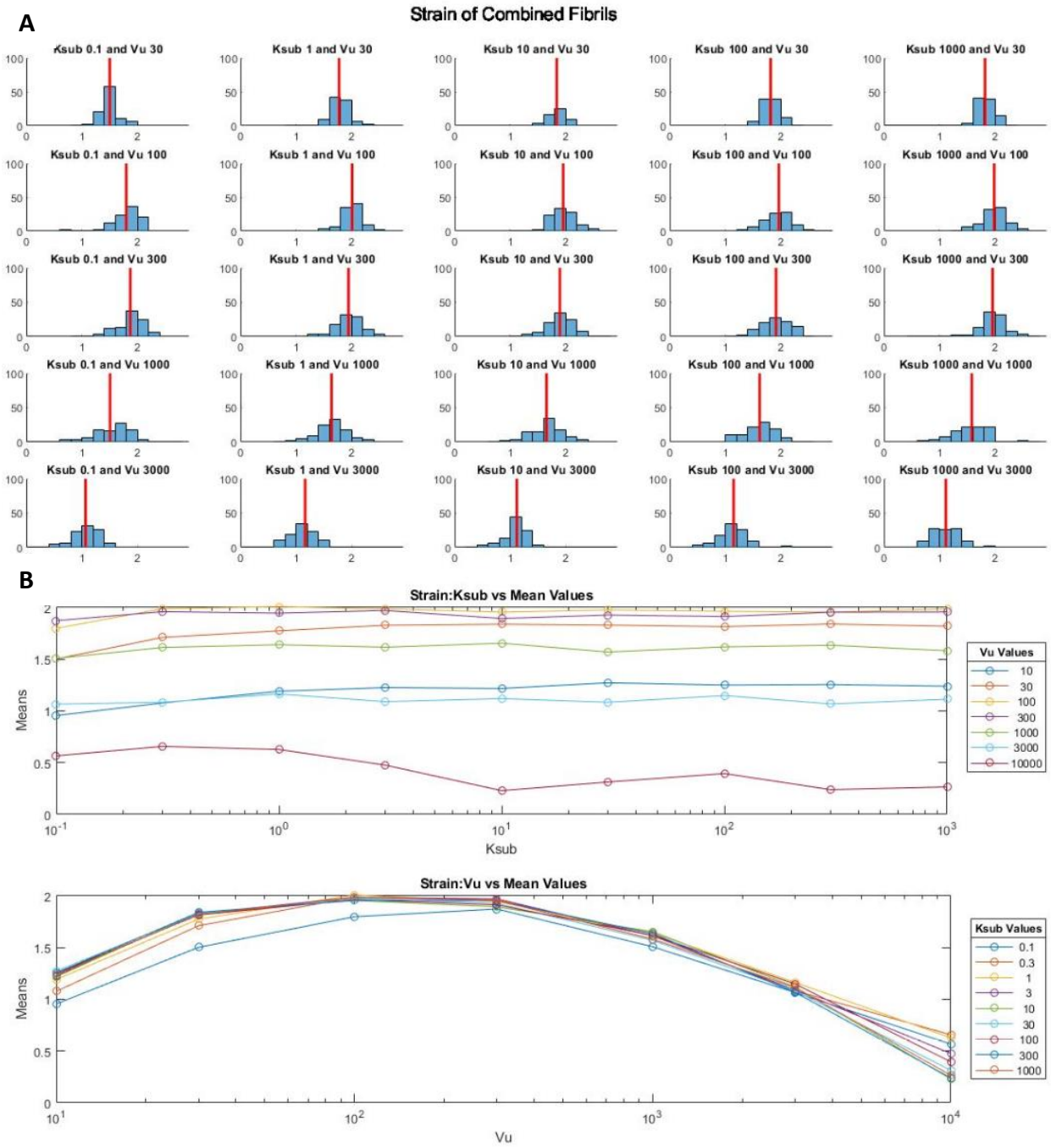

Figure 18: Results for strain for SFs. (A) Histograms showing the varying values for each unique ksub-Vu pairing. Parameter ksub of [0.1, 1, 10, 100, 1000] and parameter Vu of [30, 100, 300, 1000, 3000] were shown to observe jump in values. Red line is the mean for all simulations. (B) Line graphs showing each parameter versus the differing mean values for the property.

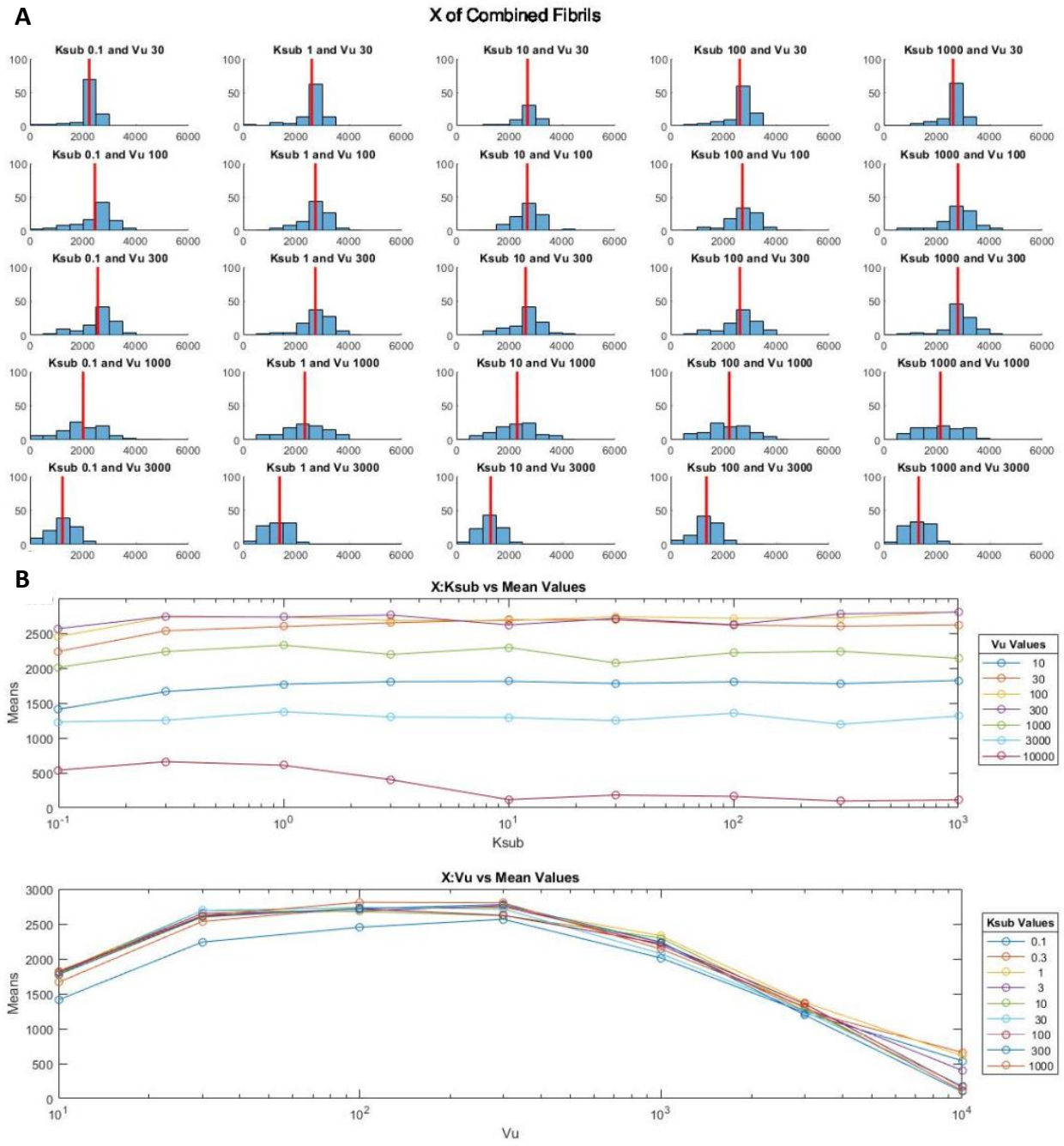

Figure 19: Results for the X (nm) for SFs. (A) Histograms showing the varying values for each unique k_{sub}-Vu pairing. Parameter k_{sub} of [0.1, 1, 10, 100, 1000] and parameter Vu of [30, 100, 300, 1000, 3000] were shown to observe jump in values. Red line is the mean for all simulations. (B) Line graphs showing each parameter versus the differing mean values (nm) for the property.

In order to observe the key differences for mean values of each property between each increase in parameter, Vu values of [10, 100, 1000, 10000] were shown in **Figures 5A-13A** and Vu values of [30, 100, 300, 1000, and 3000] were shown for **Figures 14A-19A**. **Figures 14-19** show the fibril assembly values of both SSFs and FSFs as the combined groups (SFs). These SFs are similar to the dataset of the fibril assembly for **Figures 5-13** as these datasets include the restretching capabilities for the Weinberg-Mair-Lemmon Fibronectin Model. Therefore, these results are used to answer the question for which parameter, substrate stiffness or actin velocity, determines the properties of the fibronectin assembly. After comparing all results, the actin velocity appears to have a greater affect in the development of the Fibronectin properties as shown in **Figures 5-19**. **Figures 5B-19B** show a greater difference in means with increasing Vu in comparison to k_{sub}.

When observing **Figure 5A**, the histograms with a vu value of 1000 (third row) show a greater spread of length distributions in comparison to other histograms with vu values of 10, 100 and 1000. However, there is one major thing of notice for **Figure 5B** - *k_{sub} vs Mean Values* for the line with a Vu of 10000. From a k_{sub} of 0.1 to ksub of 1, the mean stretched lengths were increasing before finally decreasing at ksub of 3. This observation can be seen for **Figures 5B-8B, 11B, 13B**. For **Figure 12B** - *k_{sub} vs Mean Values,* the Vu line of 10000 shows a considerable jump in means from k_{sub} of 3 to 10, where the mean stabilizes onwards. This would indicate that as Vu increases, the thickness of the fibril decreases at a greater rate than the stretched lengths and relaxed lengths (**Figures 5, 6, 12**). After noticing these trends and observing the rest of these results, it appears that at higher Vu values (Vu of 10000), the means values for most of

the properties appear to deviate from the rest of the Vu values for the k_{sub} *vs Mean Values* line graph. These trends involving Vu of 10000 are apparent for **Figures 5-8, 11-13, 15-19**. Another point of interest is in **Figures 9** and **10**, which involves the fraction of clutches and the total number of clutches of the fibril assembly. A great decrease in both frac and tot of clutches is observed from Vu of 100 to 1000, where at Vu of 1000, the average number of both properties is near or at zero. This indicates at high velocities after Vu of 100, the integrin bonds appear to break between the actin myosin and the fibril.

Figures 14 (substrate force for SFs)**, 18** (strain of SFs)**, 19**(X), show a parabolic increase and decrease of the property means from Vu of 10 to 300; however, **Figures 16**(slope of SFs) and **17**(stress of SFs) show the same parabolic increase and decrease for the same Vu ranges but with an increase in mean values after Vu of 3000. **Figures 14, 18, 19** signify that for those properties, an increase in Vu increases the properties up to a certain, critical point, until an increase in Vu starts to decrease these properties. For **Figures 16** and **17**, a more striking trend occurs with an addition of another increase in property means after the decrease occurs. This trend does not appear for the rest of the figures and only appears for the combined SFS and FSF data. An explanation or a pattern cannot be accurately determined until experiments can be performed with Vu values greater than 10000.

Chapter 3b: Results for Experiment 2

The second set of experiments were conducted in order to answer question 2. Do viscoelastic properties differ for different actin velocity or substrate stiffness with an example of slope of force vs displacement from rest. How do these properties differ while having different sub types of fibrils that are created during the assembly process? To answer this, a dataset containing the resulting values of the viscoelastic properties of the varying fibril assembly simulations for each sub-type, SSF and FSF, was collected in the form of .mat files.

The fibril assembly simulations were based off of the Weinberg-Mair-Lemmon model with varying parameters of k_{sub} and Vu while separating the fibril subtypes as appeared in **Figure 4**. The SSF fibrils were simulated to have integrin bonds not breaking during cell migration whereas FSF fibrils were simulated to have the integrin bonds break. Each simulation had a unique k_{sub}-Vu pairing with a k_{sub} range of: [0.1, 0.3, 1, 3, 10, 30, 100, 300, 1000], and with a Vu range of: [10, 30, 100, 300, 1000, 3000 10000]. However, in order to observe the jump in property values closely, only the Vu range of [30, 100, 300, 1000, 3000] were shown in **Figures 20A-20F.** Again, each unique parameter pairing assembly was performed again until 100 assembly simulations were created in order to reduce and possible assembly errors. Through MATLAB, the average values for each property was calculated by averaging the specific property values from the 100 simulations of a unique parameter pairing. Each property's SSF (red) and FSF (blue) fibril values were placed onto the same histogram in order to compare and contrast the two fibril types. Each histogram shows how each parameter affects the properties in both SSF subtypes and FSF subtypes to varying degrees.

A

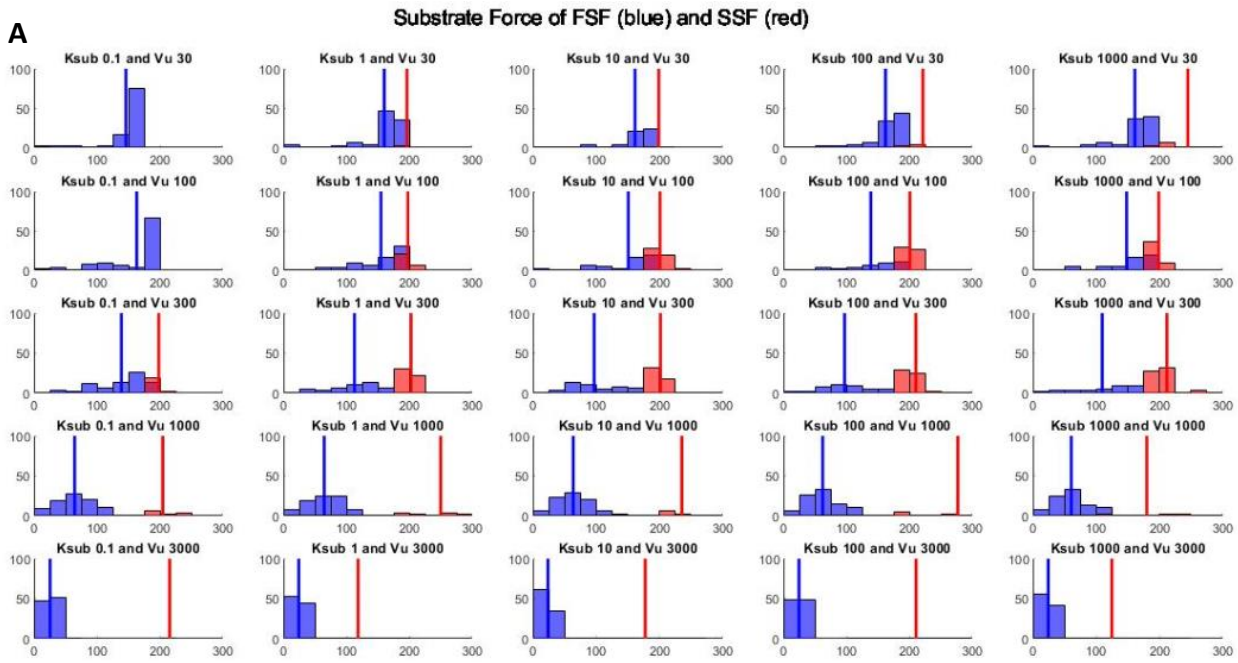

B

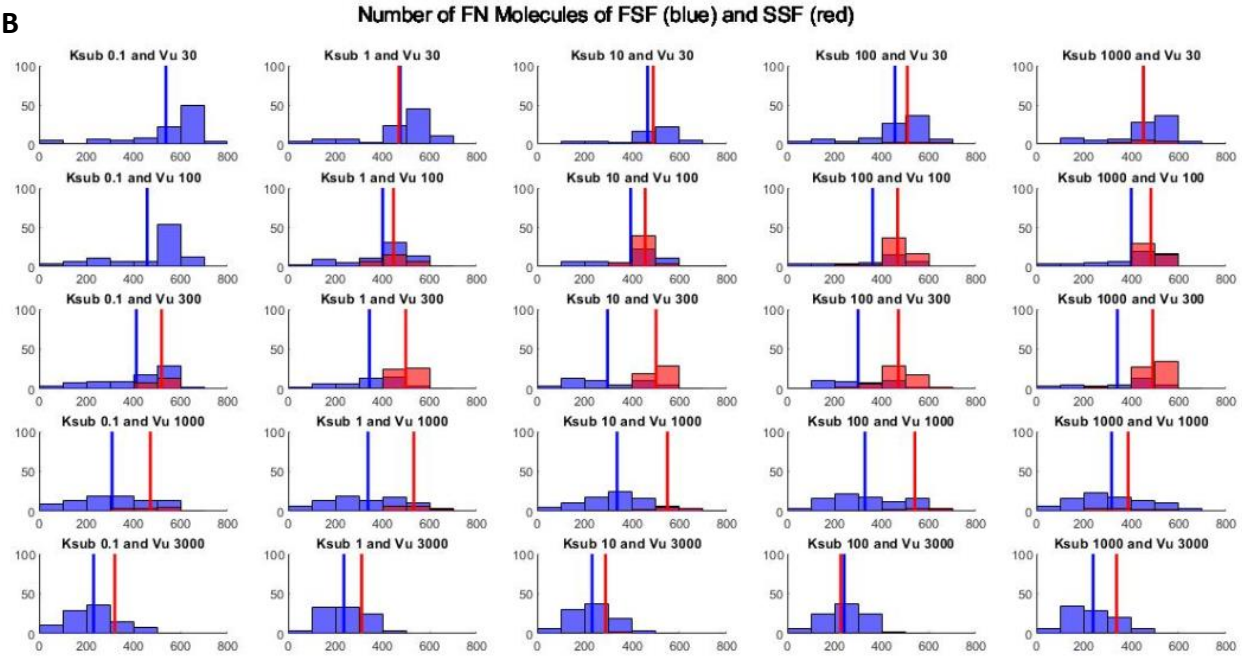

C

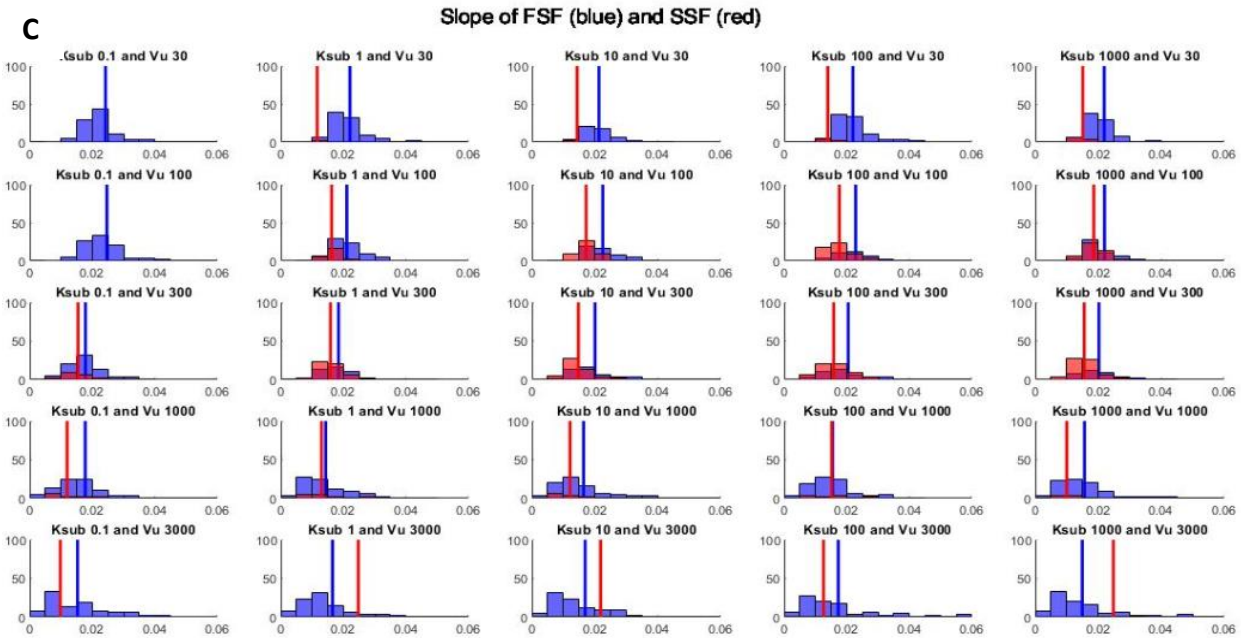

D

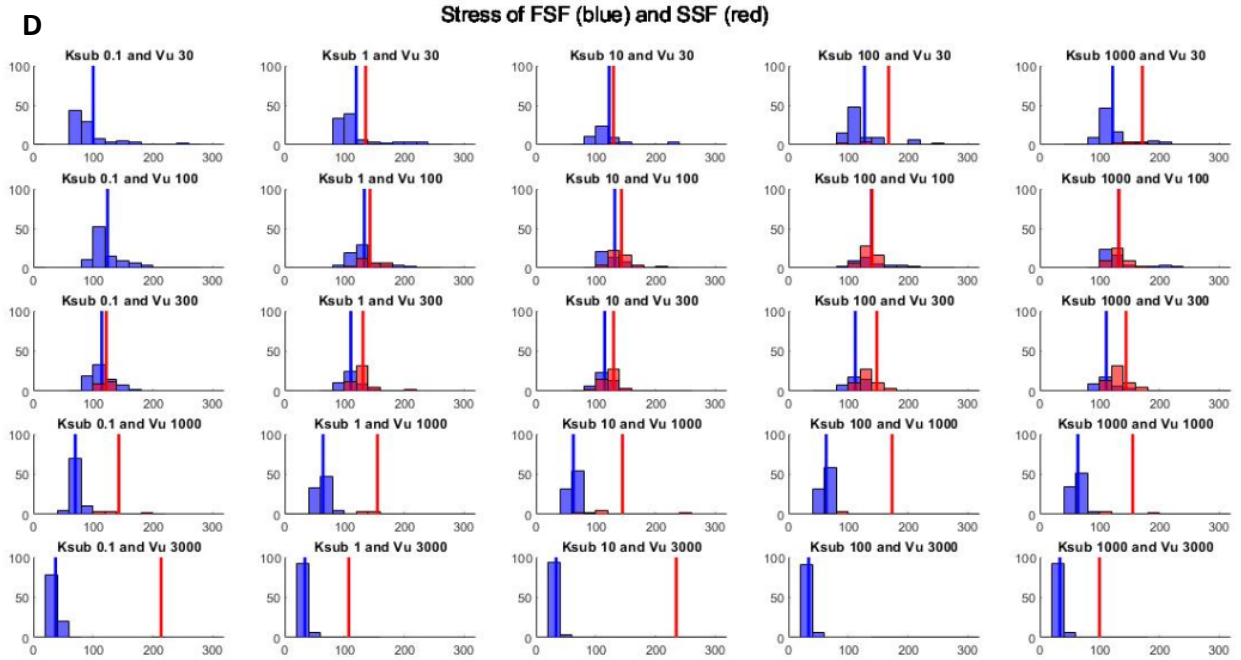

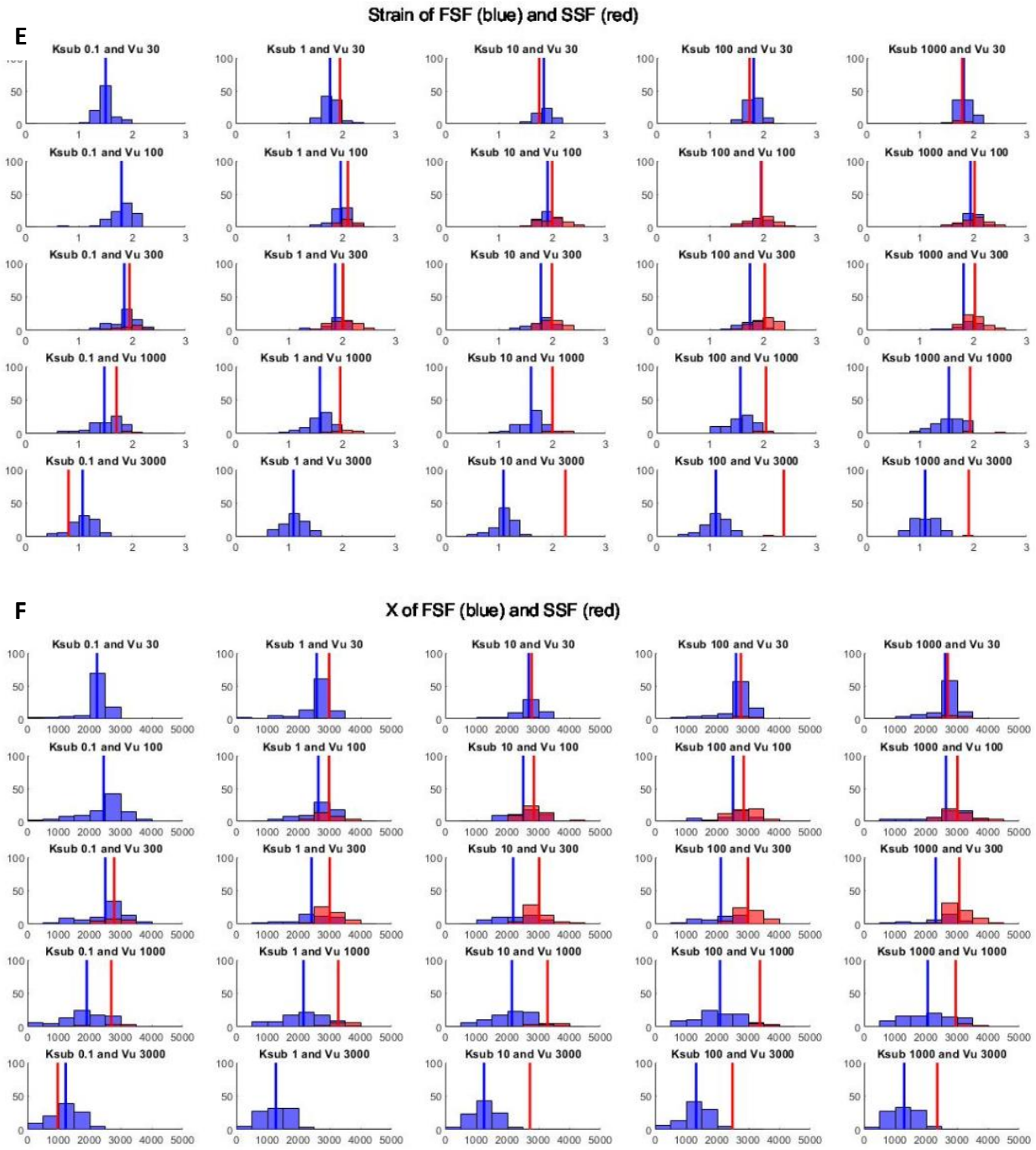

Figure 20: Histograms showing the two fibril subtype values with changes to K_{sub} and Vu. SSF (red) are labeled as terminated due to integrin bonds not restretching after breaking and FSF (blue) are labeled as not terminated due to integrin bonds being restretched after breakage. Blue vertical line - mean value for the property for the FSF subtype. Red line – mean value for the property for the SSF subtype. (A) Fsub (pN), (B) nFN, (C) Slope (pN/nm), (D) Stress (pN per nm^2), (E) Strain, (F) X (nm)

From observing **Figures 20A-F**, Vu has a greater effect on the properties of both fibril assemblies in comparison to k_{sub}. These changes can be seen for all figures. Another unique interest to note is how differently the fibril types react to the increase in Vu. **Figures 20A, B, E** show that the means of the properties for SSF fibril type greatly increases with increasing Vu and the mean for the same properties for FSF fibril type greatly decreases with increasing Vu (fsub going from 210 pN to 290 pN, etc). This pattern is observed until Vu of 3000 is reached where the mean values for SSFs decrease at the lowest and highest ksub values and increase at ksub values of 10 and 100 for **Figures 20D-E**. This observation may occur because with increasing Vu and k_{sub}, the SSF fibrils' integrin bonds break at a certain Vu and k_{sub} threshold. Additional experiments using greater Vu and k_{sub} values and pairings will be performed in order to see this threshold.

Figures 20A, B, D, E, F show that the mean values for properties for SSFs had higher mean values in comparison to properties for FSFs. **Figure 20C** (slope) shows the mean values for SSFs had lower mean values in comparison to properties for FSFs. These results are similar to the data of the Weinberg-Lemmon findings where fibril assemblies involving the SSF have constant stretching until the stall force prevents further stretching. FSFs show lower mean values due to the fact that the fibrils stretch until the integrin bonds break and the fibrils are then restretched again. **Figure 20C** is also representative of the Weinberg-Lemmon data (**Figure 4)** where the slope (resting stiffness) of the FSF assembly has a greater value than the SSF assembly. Additionally, with **Figure 20B**, it can be seen that fibrils with lower nFN appear to have slightly greater slope values in comparison to fibrils with higher nFN. In doing so, the differences between the two fibril types are noticeable not only in terms of k_{sub} and Vu, but as well in properties.

Chapter 3c: Results for Experiment 3

The third set of experiments were conducted in order to answer question 3. For a given fibril size (e.g., fibril number or resting length), how much does the viscoelastic slope from rest differ? Does this depend on actin velocity or substrate stiffness? If there are differences, how can they be explained. To answer this, the same dataset used in Chapter 3a was used again; however, the values for each property was plotted against the nFN value. The number of fibronectin molecules increases the length of the fibril size as shown in **Figure 1** and in doing so, the nFN was used as a comparison marker for fibril size. As nFN increases, the fibril size increases and seeing how this affects a particular property alongside the changes to k_{sub} and Vu can give further details to researchers if fibronectin size matters to the fibronectin matrix. The main properties that will be observed are the stretched and relaxed lengths, substrate force, and slope of the fibril assembly.

Each simulation had a unique k_{sub}-Vu pairing with a k_{sub} range of: [0.1, 0.3, 1, 3, 10, 30, 100, 300, 1000], and with a Vu range of: [10, 30, 100, 300, 1000, 3000 10000]. A Vu range of [30, 100, 300, 1000, 3000] were shown in **Figures 21A-21D** in order to see the jump in property values closely. Again, each unique parameter pairing assembly was performed again until 100 assembly simulations were created in order to reduce and possible assembly errors. Through MATLAB, the average values for each property was calculated by averaging the specific property values from the 100 simulations of a unique parameter pairing. In order to see how the fibril size affected the properties, each mean value was plotted against a range of nFN values at the time of assembly. The nFN range started with an nFN of 25 and had increments of 50 for each bin (first range starting with 25, then 75, 125, etc.).

A

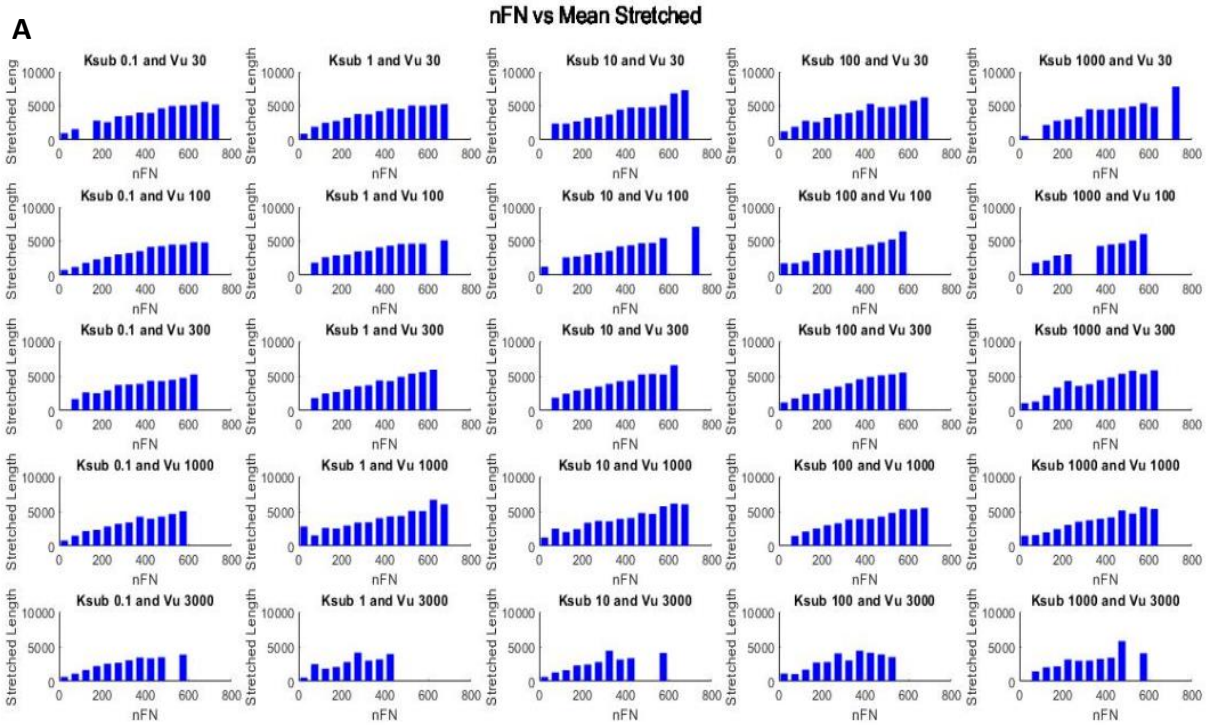

B

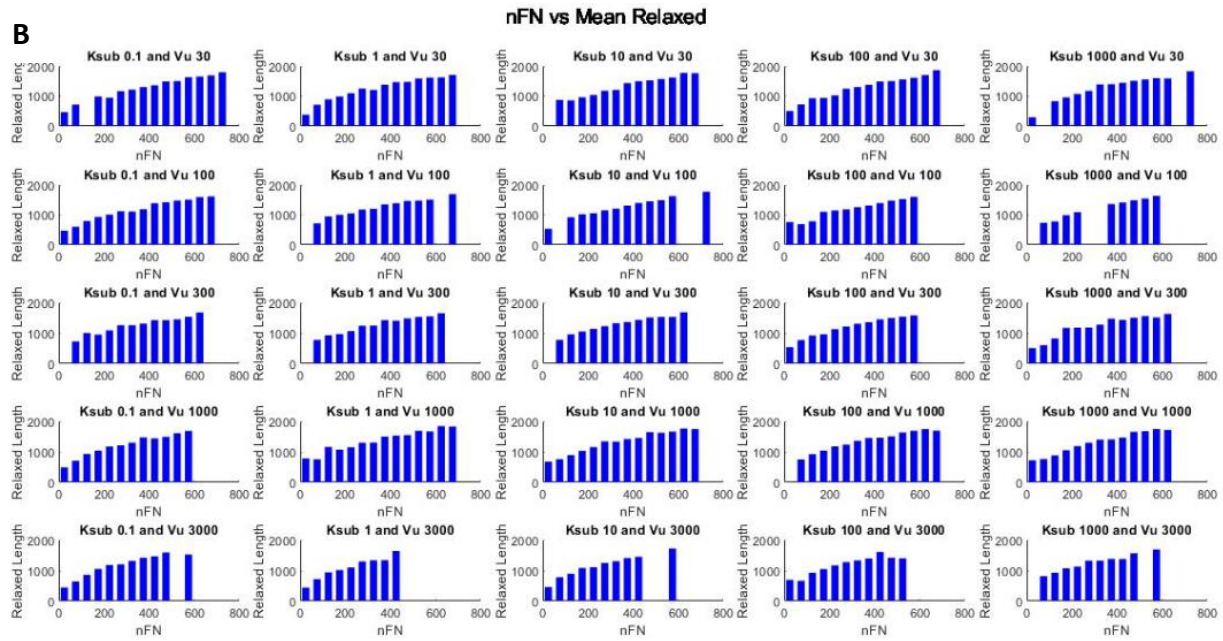

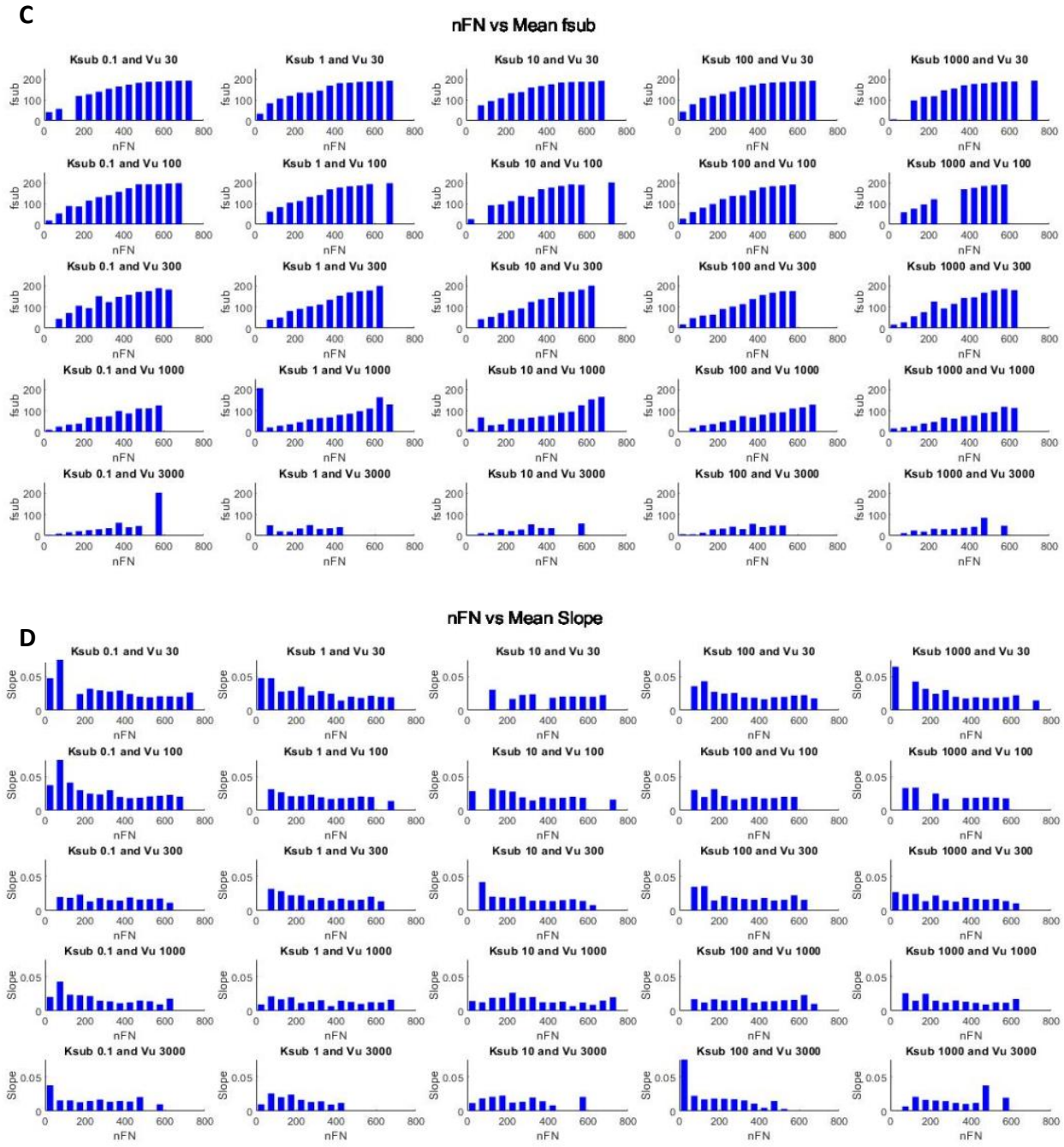

Figure 21: Histograms showing a property's mean value at its certain nFN range at during that time of assembly. (A) nFN vs mean stretched lengths (nm), (B) nFN vs mean relaxed lengths (nm), (C) nFN vs mean fsub (pN), (D) nFN vs mean slope (pN/nm).

After assembly, it appears that with an increase in nFN (fibril size) a given property's values also change. For most histograms in **Figures 21A, B, C**, an increase in fibril size (nFN) increases the mean values for stretched length, relaxed length, and fsub of the fibril. For the stretched length, length starts around 1000 nm at 25 nFN and end at a length of around 5000 nm at 775 nFN. For the same nFN bins, relaxed lengths increase from 500 nm to 2000 nm. Theoretically, this should be representative of actual fibril assemblies as with increased fibril size, the stretched length, the relaxed length, and the substrate force would increase in return. In **Figure 21D;** however, the slope seems to be affected differently with an increase in fibril size but with not as much of difference in increasing Vu. As the fibril size increases, the slope decreases from Vu of 30 to Vu of 300. Once a Vu of 1000 and 3000 is reached, the mean values for the slope start to sporadically increase and decrease with increasing nFN. As mentioned previously, the slope is determined as the change between the stretched lengths and relaxed lengths over the substrate force (X over fsub). Thus, when fibril size increases, the fsub value appears to increase at a faster rate in comparison to the stretched and/or the relaxed lengths of the fibril. The results may indicate that the stretched length and relaxed length do not increase as much to the point with increasing fibril size to the point where the difference between the two is not as great at smaller fibril sizes. Even with these observations, it is also important to note that the increase in actin velocity also changes the mean values for a given property. With increasing Vu, the mean values for all properties decrease, more noticeable at Vu of 3000. These results also indicate that increasing actin velocities cause the restretched fibrils to have their integrin bonds break.

Chapter 3d: Results for Experiment 4

The fourth set of experiments were conducted in order to answer question 4. How do cells with different actin velocities (possibly on different substrates) respond to restretching of fibrils produced by cells with a different actin velocity (and possibly substrate) and with the number of myosin motors (NM)? After performing experiments 1, 2 and 3, it became clear that substrate stiffness k_{sub} does not have as a great of an effect on determining the fibronectin's properties in comparison to Vu. However, the number of myosin motors, NM, may be an important parameter to note as myosin motors also affect fibril assembly as the motors pull on the actin filament as shown in **Figure 1**. In order to answer this, an assembly simulation was performed with NM and Vu where fibrils were restretched with differing NM and Vu combinations with an addition to varying parameters.

The fibril assembly simulations were based off of the Weinberg-Mair-Lemmon model with varying parameters of NM [30, 60, 100, 300] and Vu [30, 100, 300, 1000]. In these simulations that were performed via MATLAB, the assembly was run with one set of NM (either NM of 100 or 300) and Vu (either 300 or 1000) values. After the assembly, the fibrils were restretched with a different set of NM and Vu values. This would create four unique sets of restretched fibrils (NM of 100 and Vu of 300, NM of 300 and Vu of 300, NM of 100 and Vu of 1000, NM of 300 and Vu of 1000). Finally, the same fibrils were restretched with all of the different NM [30, 60, 100, 300] and Vu [30, 100, 300, 1000] parameter combinations. The mean values for each property for each different NM-Vu fibril and parameters combinations were collected and plotted against the corresponding parameter as shown in **Figures 22-26**.

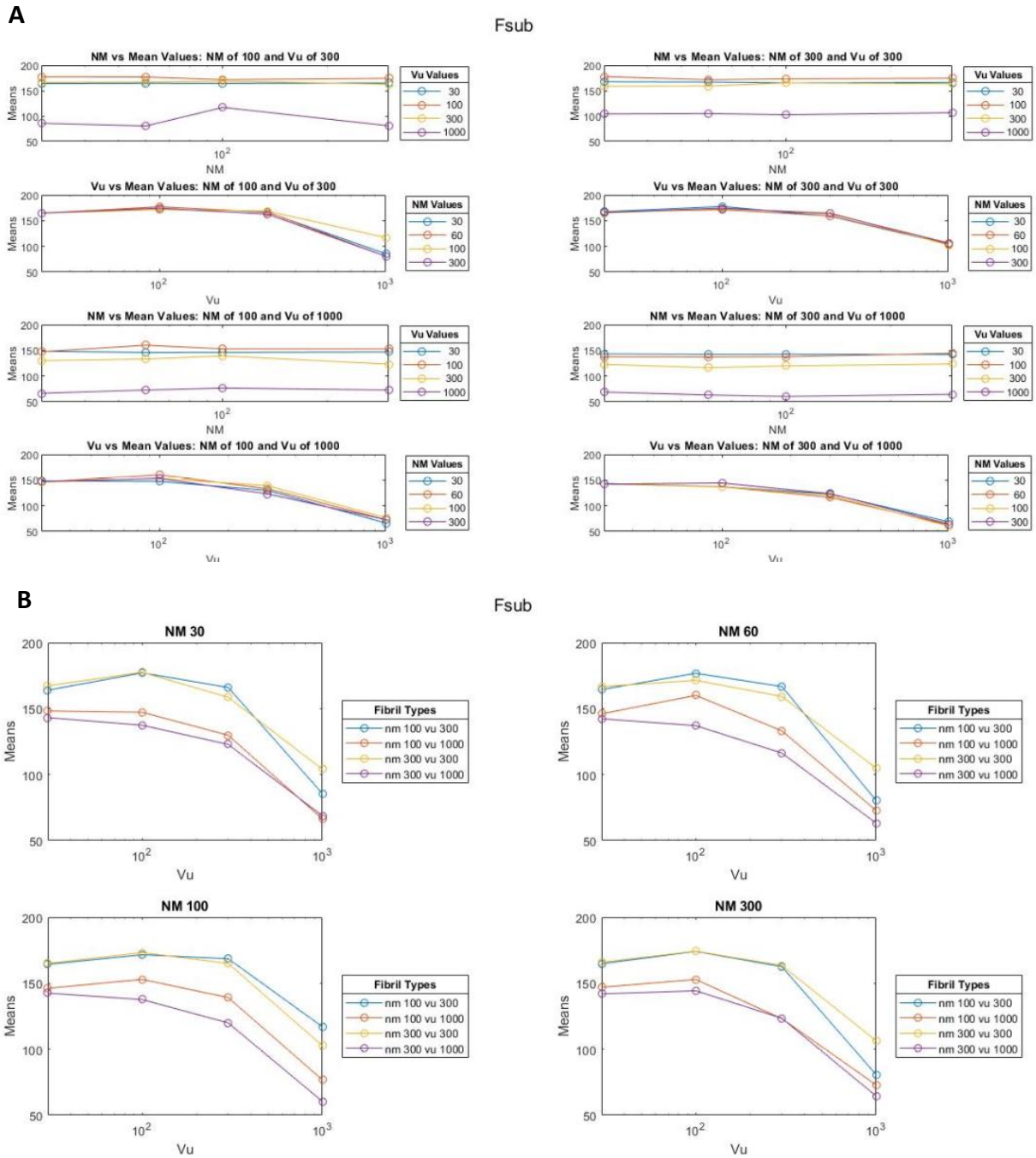

Figure 22: Mean values of fsub (pN) versus the varying parameter values of NM and Vu. (A) Line graphs comparing the four restretched fibrils while either having the mean plotted against NM or Vu. (B) Line graphs showing the mean values versus Vu while having every restretched fibril type per a given parameter value.

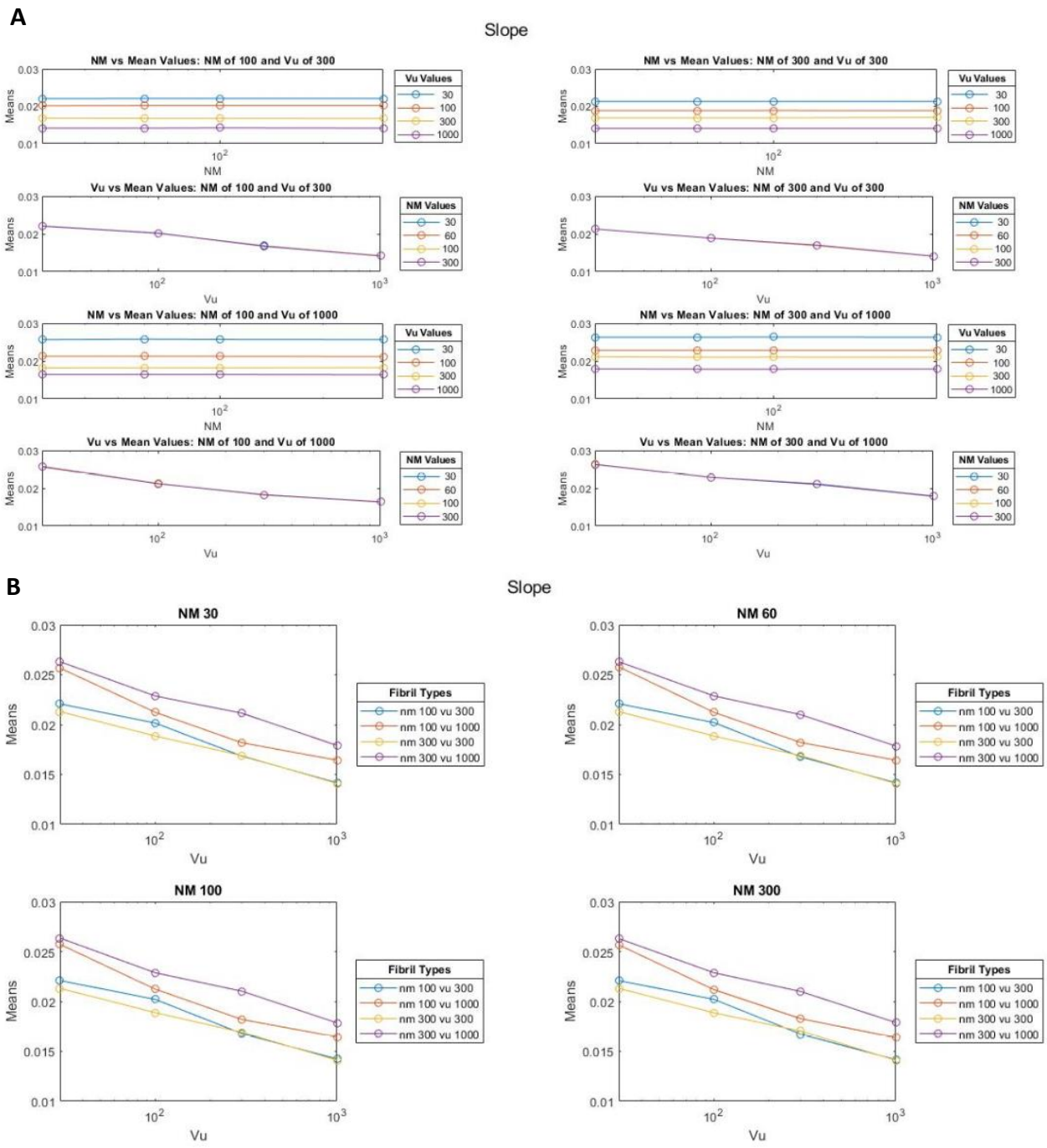

Figure 23: Mean values of the slope (pN/nm) versus the varying parameter values of NM and Vu. (A) Line graphs comparing the four restretched fibrils while either having the mean plotted against NM or Vu. (B) Line graphs showing the mean values versus Vu while having every restretched fibril type per a given parameter value.

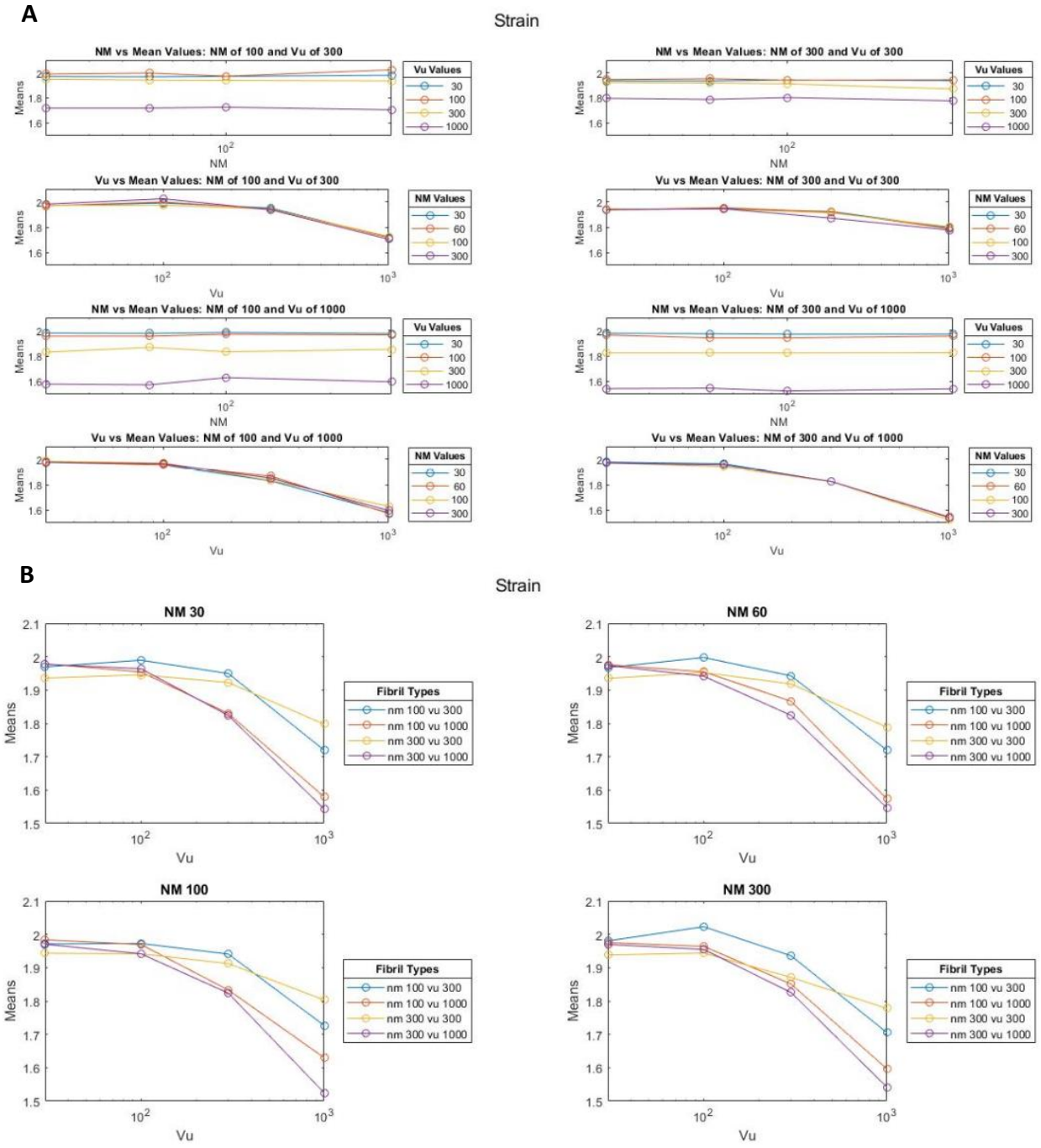

Figure 24: Mean values of the strain versus the varying parameter values of NM and Vu. (A) Line graphs comparing the four restretched fibrils while either having the mean plotted against NM or Vu. (B) Line graphs showing the mean values versus Vu while having every restretched fibril type per a given parameter value.

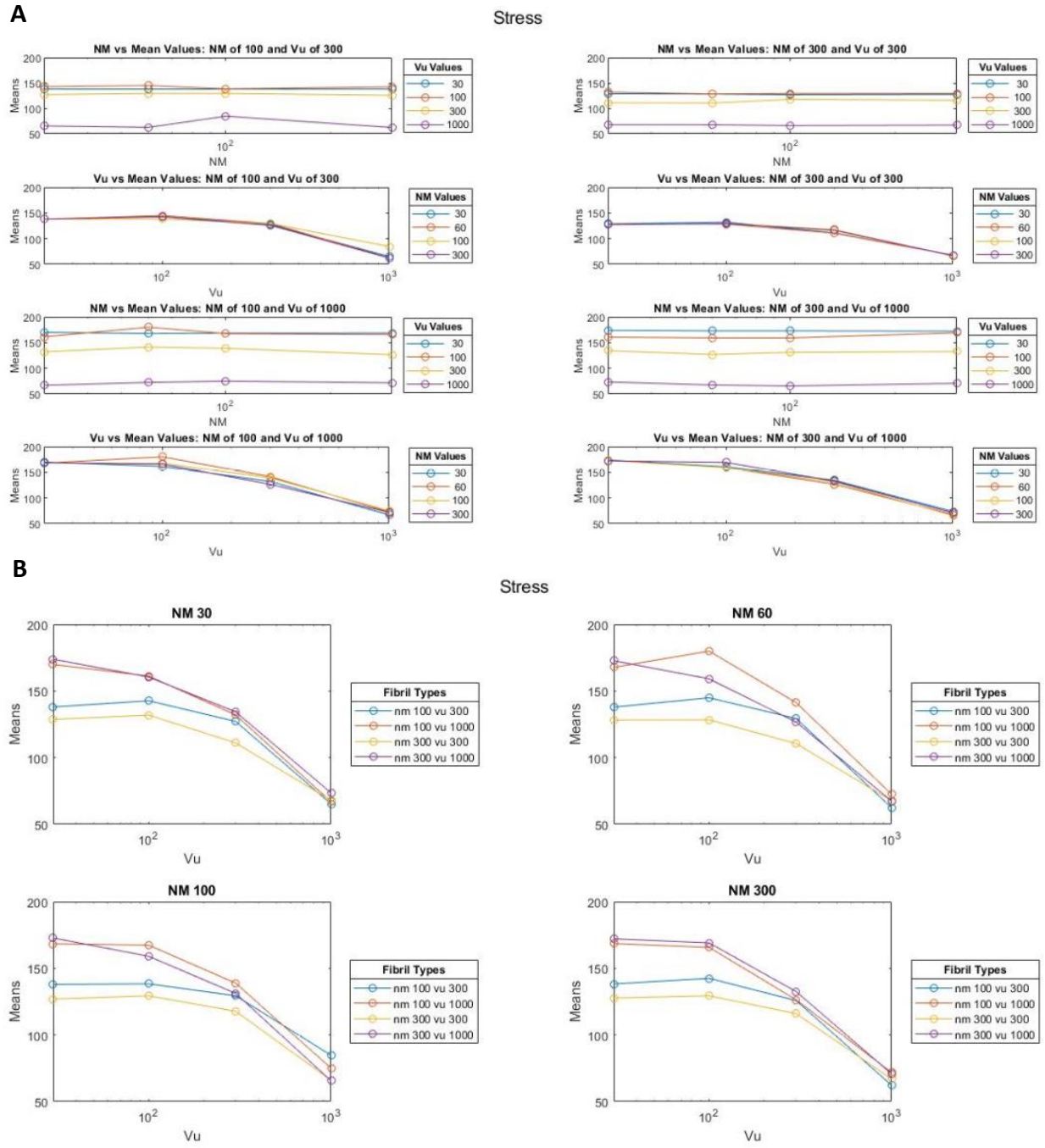

Figure 25: Mean values of the stress (pN per nm^2) versus the varying parameter values of NM and Vu. (A) Line graphs comparing the four restretched fibrils while either having the mean plotted against NM or Vu. (B) Line graphs showing the mean values versus Vu while having every restretched fibril type per a given parameter value.

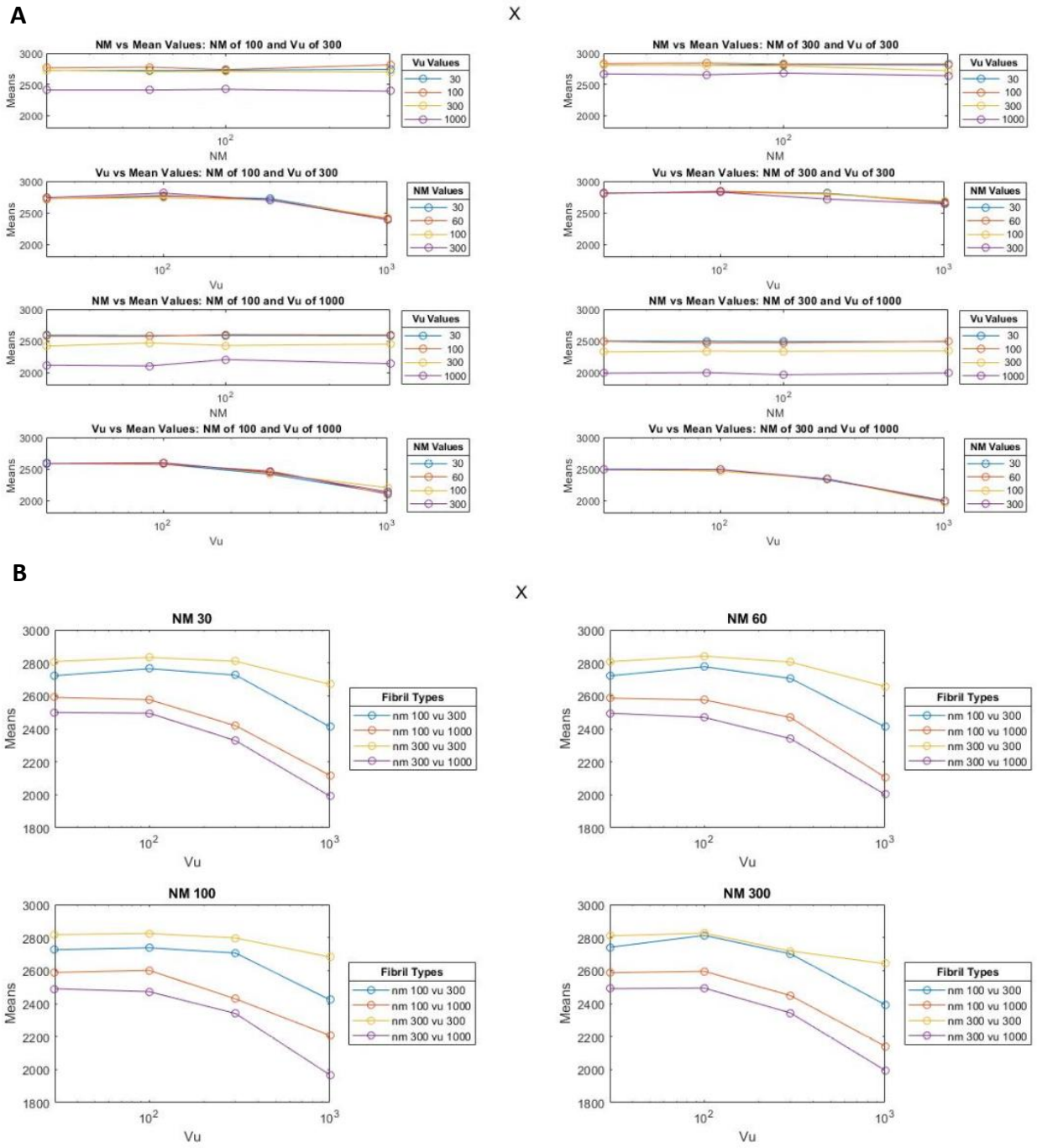

Figure 26: Mean values of X (nm) versus the varying parameter values of NM and Vu. (A) Line graphs comparing the four restretched fibrils while either having the mean plotted against NM or Vu. (B) Line graphs showing the mean values versus Vu while having every restretched fibril type per a given parameter value.

Figures 22A-26A also show that Vu affects the given property; however, the parameter NM does not affect the values for differing restretched fibrils as much as Vu. **Figures 22A-26A** - *Vu vs Mean Values* line graphs show that NM has almost zero effect on the mean values as the different fibril lines overlap one another, with the most obvious examples in **Figure 23A**. As NM increases, the mean values for the slope of the fibril stays relatively the same. This states that the number of myosin motors do have an effect on fibril assembly to some degree during the restretching process, but they do not affect the restretching of the fibril as a parameter. Fibril lines with the same Vu (blue and yellow, red and purple) appear closer together in comparison to differing Vu-NM values and same NM values. As mentioned previously, f_{stall} is a stall force dependent on the NM present for a given fibril. These results may indicate that the NM may not have much of a significance or effect on the other properties for the fibril assembly besides its ability to terminate the assembly. NM, along with k_{sub}, have given that insight of some of the parameters that are not as prevalent in the fibril assembly process as compared to Vu.

Figures 22B-26B illustrate that restretching the fibrils at differing combinations of NM and Vu does affect a given property. When a given fibril is restretched under a new Vu parameter, as Vu increases, the mean values of a given property decrease. Additionally, when fibrils are restretched, a fibrils types with the same Vu parameter before the restretching tend to be closer together in terms of mean in comparison to fibril types with different Vu values. values have greater mean values in comparison to restretched fibrils with greater Vu values. **Figures 22B**(fsub), **24B**(strain), **26B**(X) show fibrils of lower Vu (NM of 100 and Vu of 300, NM of 300 and Vu of 300) that have mean values greater than fibrils of higher Vu (NM of 100 and Vu of 1000, NM of 300 and Vu of

1000). **Figures 23B**(slope) and **25B**(stress) show the opposite with fibrils of higher Vu (NM of 100 and Vu of 1000, NM of 300 and Vu of 1000) that have mean values greater than fibrils of lower Vu (NM of 100 and Vu of 300, NM of 300 and Vu of 300). These results indicate that restretched fibrils of varying Vu do replicate the same behavior under the same conditions. To know more, the fibril size experiment that was performed in Chapter 3c was conducted again by comparing nFN to the mean at the time of assembly for the different Vu values for each NM-Vu fibril type as shown in **Figures 27A-E**.

Figures 27A-E show line graphs comparing the mean values of the five properties against nFN at varying Vu values. As Vu increases, the means of fsub, slope, strain, stress, and X decrease for each restretched fibril type. From Vu of 30 to 1000, fsub decreases from 150 to 75 pN, slope decreases from .0275 to .02, strain decreases from 2 to 1.7, stress decreases from 175 to 50 pN/nm^2, and X decreases from 2500 to 2000 nm. As nFN increase, the mean values for slope and stress decrease whereas the mean values for strain, X, and fsub increase. As mentioned previously, the values for strain, fsub and X increase as fibril size increases the length of the FN. The parameters of Vu and nFN show a great observational change to the mean values; however, the changes to the mean value is sporadic when comparing and contrasting the differing fibril NM and Vu combinations. Each restretched fibril combination (NM of 100-Vu of 300, NM of 300-Vu of 300, NM of 100- Vu of 1000, NM of 300-Vu of 1000) do not show any clear indication of how they differ from one another. Although the previous results of **Figures 22-26** do show the importance of the effects of restretching a FN matrix under different conditions; however, importance is not readily apparent in **Figures 27A-E**, but these results do signify the importance of fibril size and Vu and their effects on the fibril assembly.

A

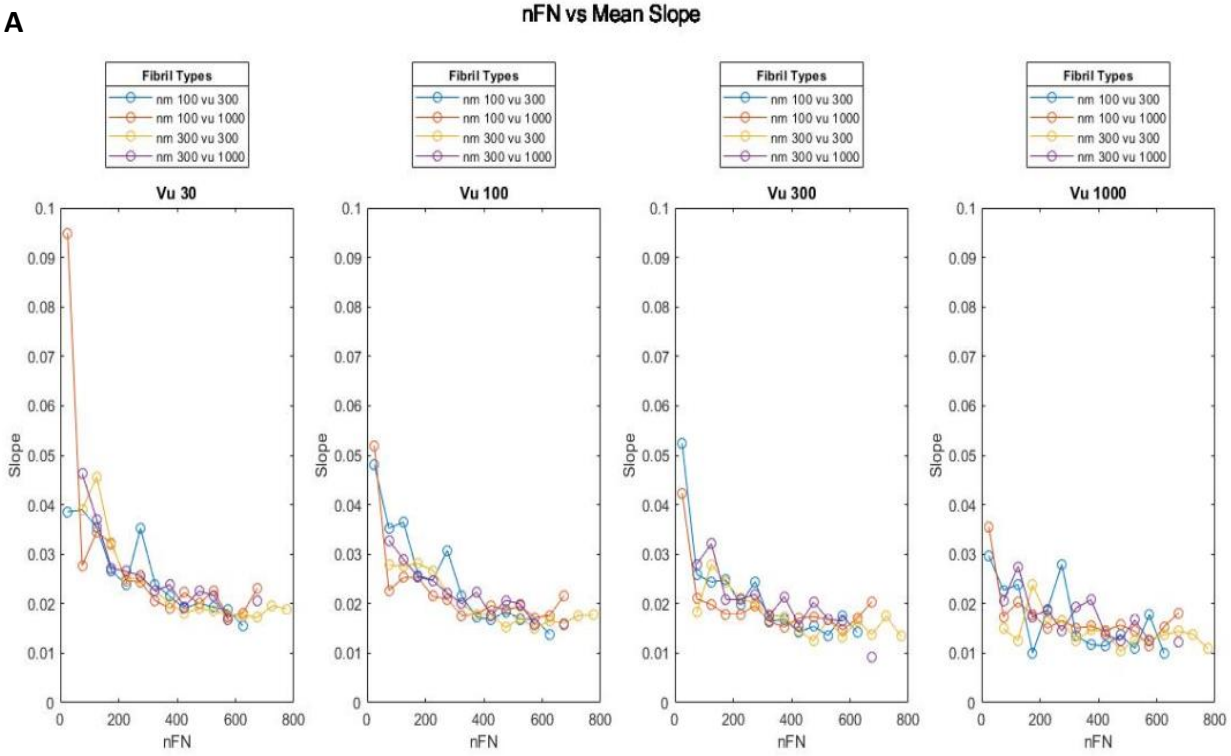

B

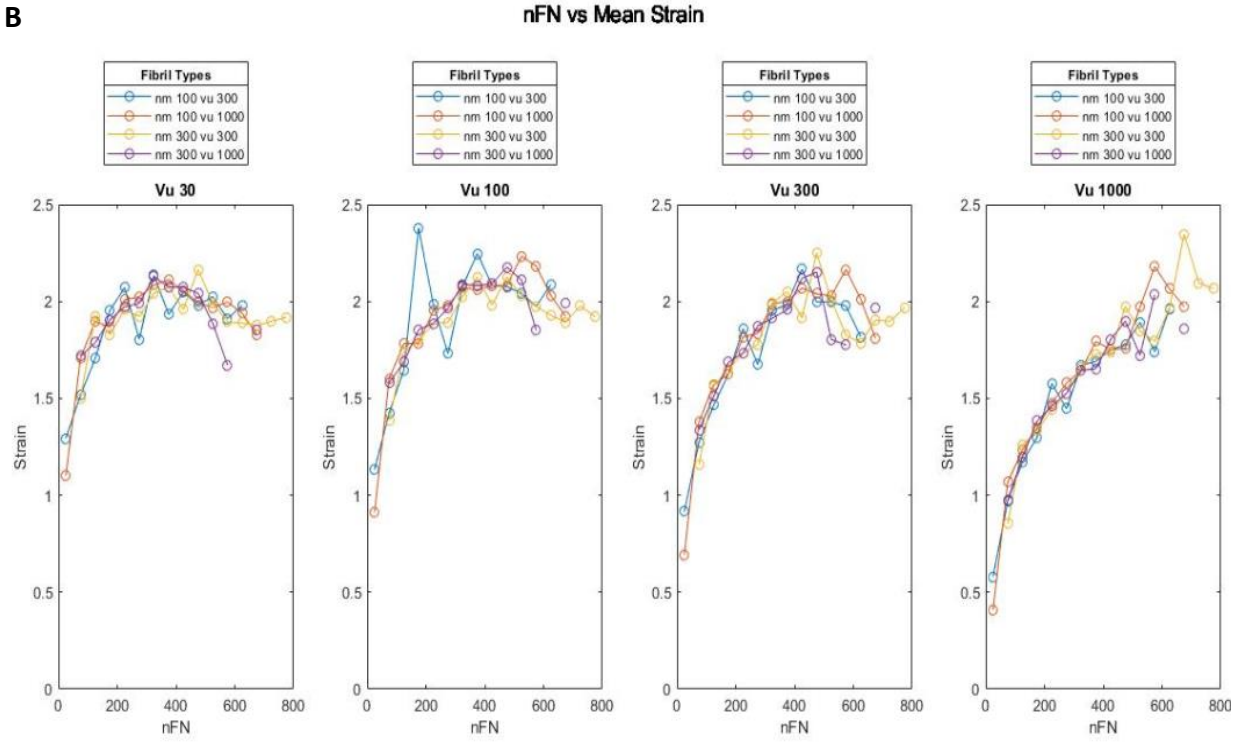

C

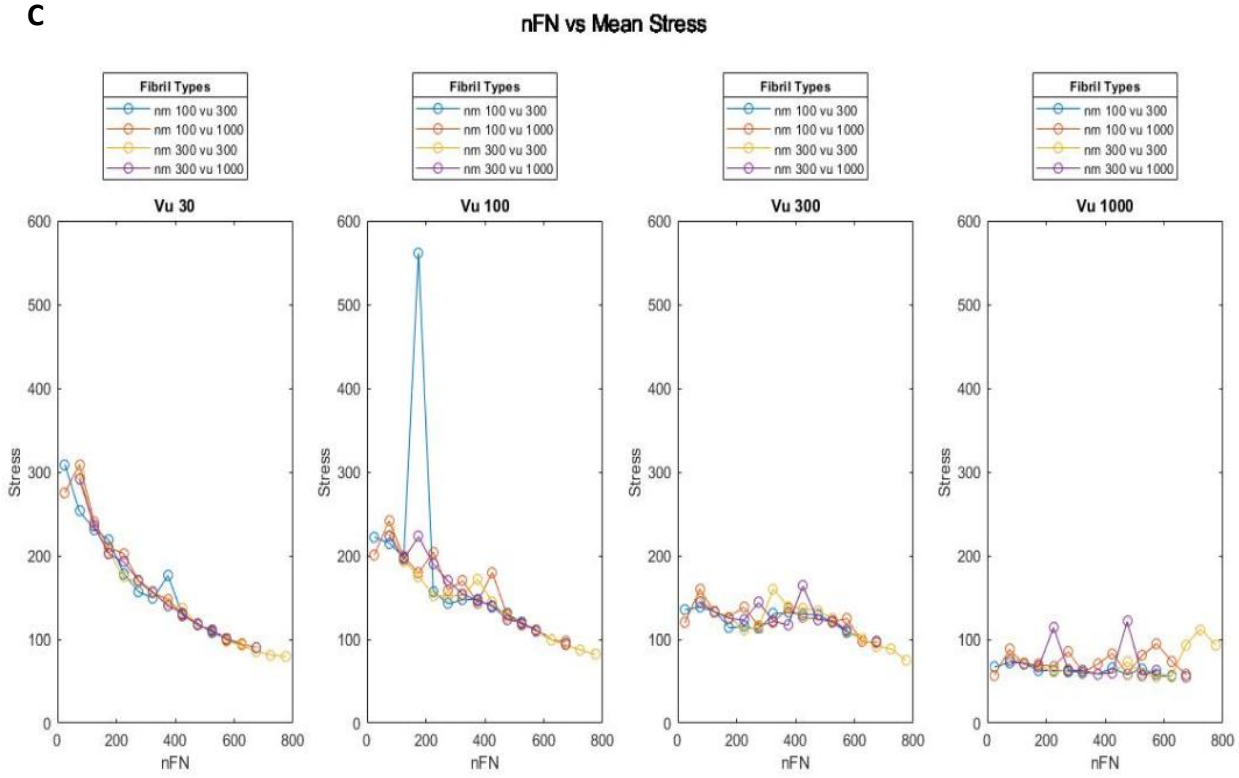

D

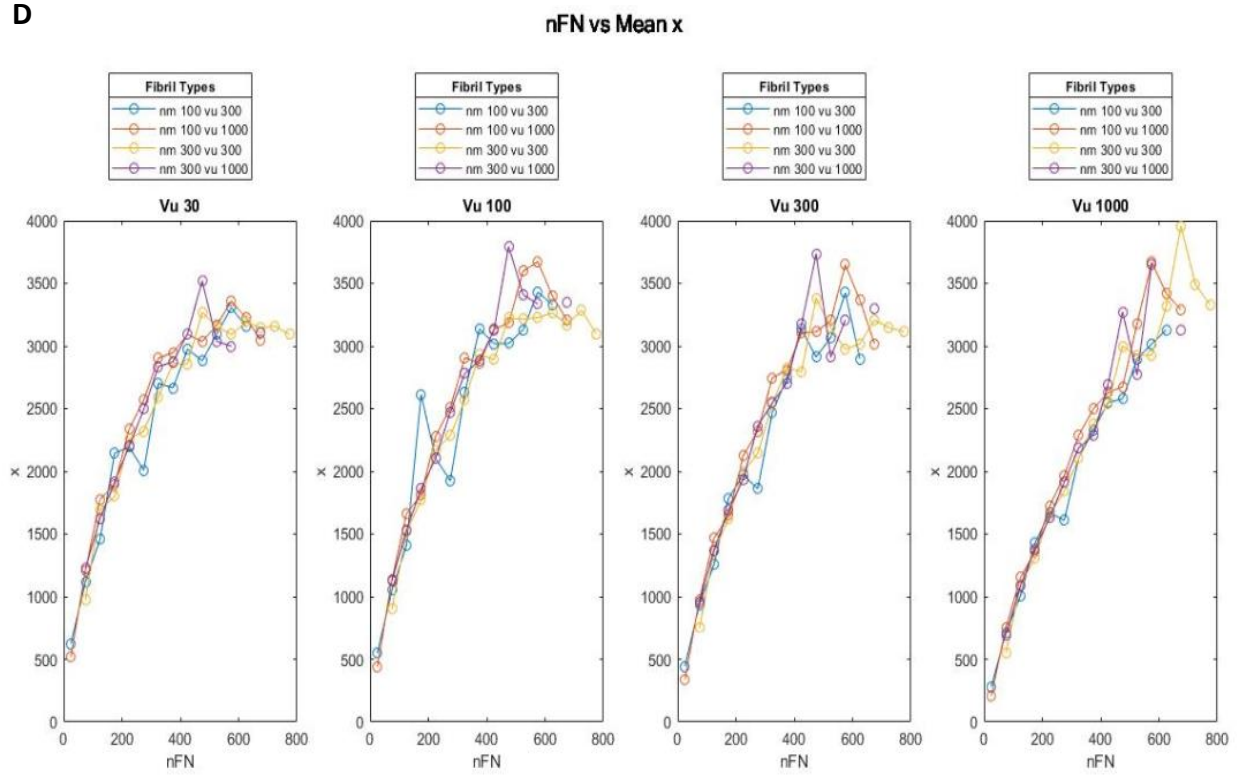

E

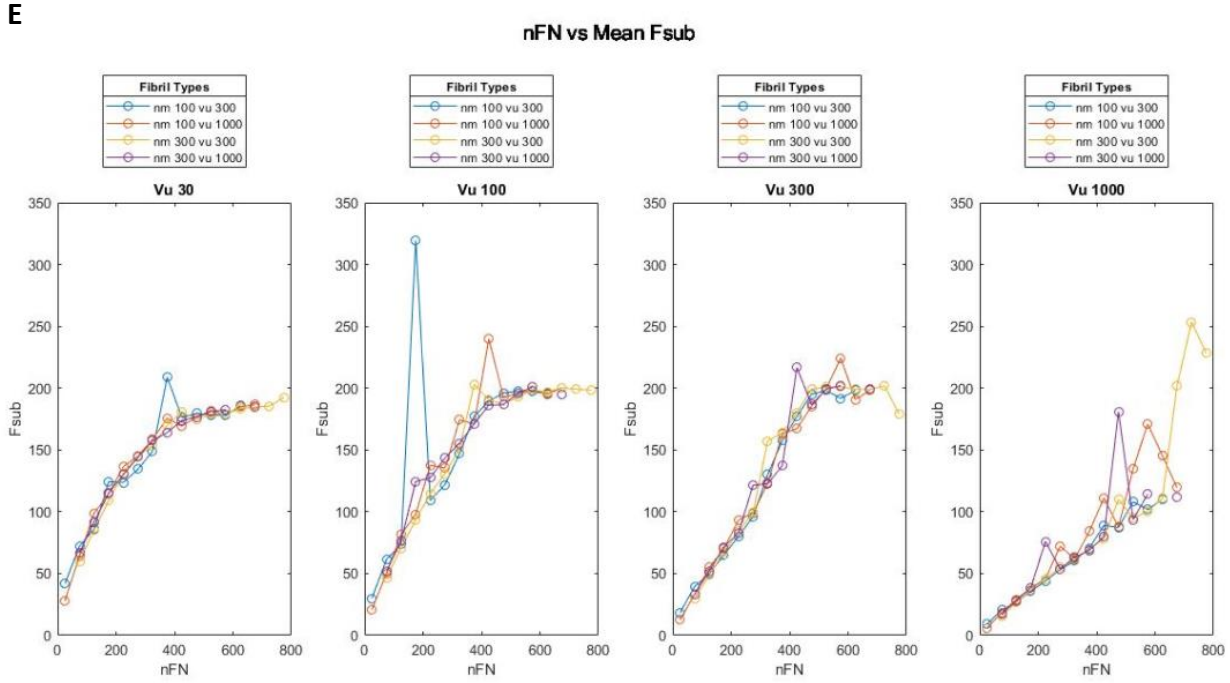

Figure 27: Line plots depicting the nFN vs the mean property value for a given NM-Vu fibril restretching combination while having different Vu paramters [30, 100, 300, 1000]. Differing Vu parameters and nFN values show changes for a given property whereas differing fibril types show no clear distinction from one another. (A) nFN vs Mean Slope of Restretched Fibrils (pN/nm), (B), nFN vs Mean Strain of Restretched Fibrils (C), nFN vs Mean Stress of Restretched Fibrils (pN per nm^2), (D) nFN vs Mean X of Restretched Fibrils (nm), (E) nFN vs Mean Fsub of Restretched Fibrils (pN).

Chapter 4: Conclusion

The purpose of this study was to understand how fibronectin is assembled and how its properties affect the fibril assembly, which in return affects the way the cell matrix operates. The Weinberg-Mair-Lemmon model was used as the basis for this simulations and studies and the simulations reproduced experimental measurements of important FN fibril properties that resemble past experiments (Weinberg et al. 2017). Knowing which variables affect the fibril assembly process is important for future exploits when dealing with fibronectin and further protein to cell communication and interactions. Through computational methods via MATLAB, simulations of fibronectin assembly were performed with varying parameters involving substrate stiffness, actin velocity, and the number of myosin motors as well observing the effects of fibril size on a given fibril matrix. After completing various simulations involving the FN assembly, it has been determined that the FN assembly is very susceptible to the influence of the actin myosin driven force, Vu, as well as fibril size (nFN). It was previously established that the substrates force, k_{sub}, is an important parameter for FN assembly as tissue stiffness has great effects on disease progression (Hayashi et al. 2015) (Brennan and Hocking 2015). However, it has been computationally determined that Vu has a greater effect on FN assembly in comparison to k_{sub}. Depending upon the property, a property either increased or decreased in value at a greater rate with an increase in Vu in comparison to k_{sub}. The stretched length (**Figure 5**) decreased in length from 5000 nm to 1000 nm when Vu increased from 10 to 10000 and the LT Ratio (**Figure 12**) increased from 30 to 40 when Vu increased from 10 to 10000. When observing from the perspective of k_{sub}, the stretched length remained around the same (with Vu of 10, stretched length remained at 5000 nm when k_{sub}

increased from 0.1 to 1000). Furthermore, fibril size does affect the fibril assembly as evidenced with properties involving stretched lengths and relaxed lengths (**Figures 21A** and **21B**) and NM does not (**Figures 22-26**).

In order to answer Question 1 to know which parameter, k_{sub} or Vu, had a greater effect on the fibril assembly, results with **Figures 5-19** were produced illustrating that fibril size and fibril properties were dependent upon Vu. It was shown in **Figures 5A, 6A**, and **7A** that when a Vu of 10000 was used to construct the fibril matrix, a noticeable decrease in mean values was observed. **Figures 9A** and **10A** show the noticeable change in mean values once the Vu value was changed from 100 to 1000, signifying that each property is affected differently at varying Vu values. **Figure 12** (LT ratio) also illustrates how the thickness of the fibril is affected with increasing Vu as stretched lengths and relaxed lengths decrease, the LT ratio increased at Vu of 1000, indicating the thickness to decrease at a considerable rate at high Vu. As seen with **Figures 16B** (slope) and **17B** (stress), a striking trend occurs with an addition of another increase in property means after an initial decrease occurs. These results indicate that further experiments will have to be performed in order to see what happens to these properties at greater Vu values. Overall, these results helped establish the basic principle that Vu is a greater determining factor in affecting fibril assembly in comparison to k_{sub}; however, properties are affected at different rates of increase or decrease at different levels of Vu, indicating another point of interest to experiment and elaborate.

In order to answer Question 2, to know how Vu and k_{sub} affect different fibril assemblies, results with **Figures 20A-F** were produced to highlight the difference between SSFs (fibrils that were constantly stretched until f_{stall} was reached) and FSFs

(fibrils that were stretched repeatedly after the FN's integrin bonds break). These results showed that not only the different fibril types were affected by varying levels of Vu, but as well as showing how each fibril type differed from one another at the same k_{sub}-Vu pairing. Once the Vu of 3000 is reached, mean values for SSFs start to decrease at the lowest and highest ksub values and increase at ksub values of 10 and 100 for **Figures 20D** and **20E**. This observation may occur due to the fact that with increasing Vu and k_{sub}, the constantly stretched SSF fibrils may break at a certain Vu and k_{sub} threshold; which points for further experiments involving greater Vu and k_{sub} values in order to see if a threshold exists. Additionally, these results mimic the results that were observed for the Lemmon and Weinberg group involving the same fibril types with some of the same properties (Lemmon and Weinberg, 2017). In doing so, new, important observations were discovered in regard to seeing how the SSF and FSF fibrils differed from one another.

In order to answer Question 3, results with **Figures 21A-D** were shown to illustrate that in terms of fibril size (number of FN molecules from small to large), most properties showed that fibril size is not influenced by k_{sub} but by Vu. Each histogram showed similar bar sizes and distributions in **Figures 21A-D** across the k_{sub} variations; however, Vu had a great influence at higher Vu values as seen for properties involving fsub and slope. Importantly, the properties of stretched length, relaxed length, slope, and fsub were mainly tested for as these properties were correlated with one another (the difference between the stretched length and relaxed length over fsub is equal to the slope of the fibril as shown in **Figure 4B**). After observing all four figures, as fibril size increases, the fsub increased at a faster rate in comparison to the stretched and/or the relaxed lengths of the fibril. This means that the stretched length and relaxed length do not increase at a

rate comparable to the fsub when placed under observations involving increasing fibril size to the point where the difference between the two is not as great at smaller fibril sizes. Nonetheless, both Vu and fibril size play a key role in helping to shape fibril assembly as both components showed results that depicted changes to the mean values for each property with differing Vu values and fibril sizes.

In order to answer Question 4, results with **Figures 22-26** as well as **Figures 27A-E** were produced to see how NM, Vu, and fibril size affected fibrils that were restretched under different NM and Vu values. Overall, these results show observations regarding to what would happen if a fibril assembly were to be restretched with different parameter pairings. Fibrils with lower Vu values that were restretched again have shown to have higher mean values for a property in comparison to fibrils with higher Vu values. This in return indicates that if cell were to restretch a given fibril again with different actin velocity values or with different parameter pairings, the fibril will have its properties be affected. This can lead to further fibril assembly experiments in the future where mechanical stimuli can be replicated as varying cell types that restretch the fibronectin under different conditions. It is possible that under *in vivo* conditions, a cell that restretched the FN can have different number of number of myosin motors and different actin velocities that pulls on the FN. In doing so, these results show potential in creating further experiments that uses fibril assembly simulations under various restretching stages.

After obtaining results that explained the nature of both parameters and properties, it became evident on what factors help influence and shape the fibronectin matrix and the fibril assembly process. Although these experiments did help to illustrate some aspects of the fibril assembly, there is much more needed work to be done in order to grasp a

greater understanding of the mechanical signaling performed in cells. The FN assembly is just a part of a greater area of research in terms of mechanical signaling and mechanotransduction research. Fibronectin fibrillogenesis is needed for the ECM as relaxed fibronectin fibrils serve as templates for the assembly of collagen 1 fibrils, which in return, protect fibrils from being stretched by cellular traction forces (Theocharis et al 2019). The ECM provides chemical and mechanicals signals to cells and these interactions are important for research relating to cancer cells as the development of these disease are associated to the way the ECM is modeled, including the way the fibronectin matrix is formed.

The study performed here somewhat limits the way the cell signaling is looked at based upon what happens to the FN assembly when a few parameters is changed and how these changes affect certain properties of the FN matrix. The FN assembly is a core part of the ECM, and in depth, the mechanical events that occur between the ECM and the surrounding tissue. The main parts for mechanotransduction that is observed in this study only show the molecular signaling events for the FN matrix and not for entire ECM assembly. Even though this point is made; however, developing further insight about the FN assembly how it is influenced by various changes through actin velocity, substrate stiffness, fibril size, and restretching of different fibril types is still equally important. By understanding the micro-events that can occur with FN assembly, future experiments can be performed by changing some variables and parameters of the FN assembly how these changes can impact ECM and other cell related signaling pathways. The FN assembly and fibril matrix not only can affect the surrounding cells and tissue of a given area, but as well as cellular responses and signaling cascades, such as for platelet derived growth

factors (Farrar and Hocking, 2018). Due to these understandings, further experimentation would like to be performed in order to see how changes to the FN assembly can affect the surrounding cells as well as other areas of interest. Overall, the FN assembly and its mechanotransduction process are just smaller parts of a bigger picture that can help us understand the mechano-cellular interactions that can occur between cells and the ECM.

References

Lemmon, C. and S. Weinberg. Multiple Cryptic Binding Sites are Necessary for Robust Fibronectin Assembly: An *In Silico* Study. *Scientific Reports* 7, 18061 (2017).

Weinberg, S., D. Mair, and C. Lemmon. Mechanotransduction Dynamics at the Cell-Matrix Interface. *Biophysical Journal* 112, 1962-1974 (2017).

Clark RA, et al. Fibronectin and fibrin provide a provisional matrix for epidermal cell migration during wound reepithelialization. *J Invest Dermatol*. 79, 264–9. (1982)

Schwarzbauer JE, W. DD. Fibronectins, their fibrillogenesis, and *in vivo* functions. *Cold Spring Harb Perspectives Biology*. 3: a005041 (2011).

Holmes DF, Lu Y, Starborg T, and Kadler KE. Collagen Fibril Assembly and Function. *Current Topics in Developmental Biology* 130:107-142 (2018).

Singh P, C. Carraher, and JE Schwarzbauer. Assembly of Fibronectin Extracellular Matrix. *Annu Rev Cell Dev Biol*. 26:397-419 (2013).

Ruoslahti E, Obrink B. Common principles in cell adhesion. *Exp Cell Res*. 227:1–11. (1996).

Xu J, Bae E, Zhang Q, Annis DS, Erickson HP, Mosher DF. Display of cell surface sites for fibronectin assembly is modulated by cell adherence to 1F3 and C-terminal modules of fibronectin. PLoS One. 4:e4113. (2009).

Mosher DF, Fogerty FJ, Chernousov MA, Barry EL. Assembly of fibronectin into extracellular matrix. *Ann N Y Acad Sci.* 614:167–80. (1991).

Mao Y, Schwarzbauer JE. Fibronectin fibrillogenesis, a cell-mediated matrix assembly process. *Matrix Biol.* 24:389–99. (2005).

Barker TH, Engler AJ. The provisional matrix: setting the stage for tissue repair outcomes. *Matrix Biol.* 60–61:1–4. (2017).

Muro AF, Chauhan AK, Gajovic S, Iaconcig A, Porro F, et al. Regulated splicing of the fibronectin EDA exon is essential for proper skin wound healing and normal lifespan. *J Cell Biol*. 162:149–60. (2003).

Sakar MS, Eyckmans J, Pieters R, Eberli D, Nelson BJ, Chen CS. Cellular forces and matrix assembly coordinate fibrous tissue repair. *Nat Commun*. 7:11036. (2016).

Cuda G, E. Pete, R. Cooke, JR Sellers. In Vitro Actin Filament Sliding Velocities Produced by Mixtures of Different Types of Myosin. *Biophysical Journal* 72: 1767-1779. (1997).

Berg W.A., Mendelson E.B., Cohen-Bacrie C. Quantitative maximum shear-wave stiffness of breast masses as a predictor of histopathologic severity. AJR Am. J. Roentgenol. 205:448–455 (2015).

Bangasser B.L., Rosenfeld S.S., Odde D.J. Determinants of maximal force transmission in a motor-clutch model of cell traction in a compliant microenvironment. Biophys. J. 105:581–592 (2013).

Chan C.E. and Odde D.J. Traction dynamics of filopodia on compliant substrates. Science. 322:1687–1691 (2008).

Lemmon C.A., Chen C.S., Romer L.H. Cell traction forces direct fibronectin matrix assembly. Biophys. J. 96:729–738 (2009).

Fu J., Wang Y.K., Chen C.S. Mechanical regulation of cell function with geometrically modulated elastomeric substrates. Nat. Methods. 7:733–736. (2010).

Hayashi M., Yamamoto Y., Iwase H. Associations between elastography findings and clinicopathological factors in breast cancer. Medicine. 94:e2290. (2015).

Brennan JR, Hocking DC. Cooperative effects of fibronectin matrix assembly and initial cell-substrate adhesion strength in cellular self-assembly. *Acta Biomater*. 32:198-209. (2015).

Theocharis AD, Manou D, and Karamanos NK. The extracellular matrix as a multitasking player in disease. *The FEBS Journal*. 1-40 (2019).

Farrar CS and Hocking DC. Assembly of fibronectin fibrils selectively attenuates platelet-derived growth factor-induced intracellular calcium release in fibroblasts. *Journal of Biological Chemistry* 293:48. (2018).

Vita

Navpreet Singh Saini was born on May 21, 1995 in Peel Region, Brampton, Ontario, Canada. He later moved to Virginia, United States of America and earned his American citizenship. He graduated with Biotech Certification from Osbourn Park High School in Prince William County, Manassas, Virginia in 2013. He earned his Bachelor of Science Degree in Bioinformatics at Virginia Commonwealth University, Virginia in 2016. He worked at the United States Department of Agriculture for a while, while earning his Master's Degree in Biomedical Engineering at Virginia Commonwealth University, Virginia.